Synthesis, Spectroscopy, and Electrochemistry of Tetra-*tert*-butylated Tetraazaporphyrins, Phthalocyanines, Naphthalocyanines, and Anthracocyanines, together with Molecular Orbital Calculations

Nagao Kobayashi,*[a] Shin-ichiro Nakajima,[b] Hiroshi Ogata,[a] and Takamitsu Fukuda[a]

Abstract: Tetraazaporphyrins (TAPs), phthalocyanines (Pcs), naphthalocyanines (Ncs), and anthracocyanines (Acs) with four *tert*-butyl groups attached at similar positions have been synthesized, and their electronic absorption, magnetic circular dichroism (MCD), IR, and voltammetric properties were studied and interpreted with the help of quantum-mechanical calculations. Through the preparation of a series of compounds with the same number of the same substituent, the effects of the increase in the size of the ring system were clearly derived. The main results may be summarized as follows. 1) The Q band shifts to longer wavelength and its intensity increases, but with decreasing degree of change with increasing molecular size. If the size of the effect of benzene directly fused to the TAP skeleton is set at unity, the effects of the second and third benzene units are roughly 0.8 and 0.5, respectively. 2) The splitting of the Q bands in metal-free compounds decreases with increasing molecular size, so that the Q bands of H_2Nc and H_2Ac appear as single bands. 3) The magnitude of the orbital angular momentum of the excited state of the ligand decreases with increasing molecular size. 4) Interestingly, the ring current, as judged from the positions of pyrrole proton signals in the ^{1}H NMR spectrum, appears to decrease with increasing molecular size. 5) The first reduction potential becomes less negative, but only slightly, whereas the first oxidation potential shows a marked shift to less positive values with increasing molecular size, indicating that the HOMO destabilizes significantly as the molecule becomes larger. 6) In 5), the extent of the HOMO destabilization with molecular size differs depending on the central metal, so metals producing smaller destabilization effects can allow larger macrocycles. Of the metals studied, the most effective is cobalt, and the practical size limit is represented by the Acs. 7) The IR spectra become simpler the larger the molecule, and the main bands were assigned by DFT calculations. 8) The trend in experimentally determined redox potentials and electronic absorption and MCD spectra were reasonably reproduced by MO calculations using the ZINDO/S Hamiltonian. 9) EPR data for several metallocomplexes are also reported.

Keywords: density functional calculations · electrochemistry · IR spectroscopy · phthalocyanines · UV/Vis spectroscopy

Introduction

Phthalocyanines (Pcs) and porphyrins attracted the attention of many researchers during the twentieth century and are still being actively studied into this century. As a result, many monograph series on these compounds have been published,[1,2] and the International Society of Porphyrins and Phthalocyanines was established in 2000.[3] Of these compounds, Pcs are of enormous technological importance for the manufacture of blue and green pigments and as catalysts for removal of sulfur from crude oil.[2b,c,4] Other areas of interest in a variety of high technology fields[5]—such as for use in semiconductor devices, photovoltaic and other types of solar cell, electrophotography, rectifying devices, molecular electronics, electrochromic display devices, low-dimensional metals, gas sensors, liquid crystals, nonlinear optics, and photosensitizers and deodorants[4]—have stimulated research into Pc congeners such as TAPs and Ncs, particularly over the last decade. Pcs are often more suitable than porphyrins for several purposes. For example, they can be mass-produced from more economical materials, often in only a few steps in moderate to high yields, and are more

[a] Prof. Dr. Dr. N. Kobayashi, Dr. H. Ogata, Dr. T. Fukuda
Department of Chemistry, Graduate School of Science
Tohoku University, Sendai 980–8578 (Japan)
Fax: (+81) 22-217-7719
E-mail: nagaok@mail.tains.tohoku.ac.jp.

[b] Dr. S.-i. Nakajima
Meiji Pharmaceutical University, Noshio 2-522-1
Kiyose, Tokyo 204–8588 (Japan)
Fax: (+81) 424-95-8779

DOI: 10.1002/chem.200400275

versatile and robust than porphyrins. In addition, adjustment of the color, which is important for recent applications, is not difficult, since many substituents that affect electronic structure can generally be introduced onto the periphery of the ligand fairly readily, and this is reflected in the Q band position and intensity in the visible region.[6–8] However, the effect of increasing the size of the ring system has not been explicitly and quantitatively reported, because of the lack of a series of compounds possessing corresponding numbers of the same substituents. To extract properties intrinsic to the enlargement of the ring system as quantitatively as possible, we have prepared tetraazaporphyrins (TAPs), phthalocyanines (Pcs), naphthalocyanines (Ncs), and anthracocyanines (Acs), each with four *tert*-butyl groups at similar positions (Scheme 1), reducing ambiguities in analysis, which makes our compounds ideal for the purpose of the present study. Their spectroscopic and electrochemical properties have been compared, and some of the results were interpreted on the basis of quantum-mechanical calculations. Since these compounds have commercial applications, the data collected in this paper should be useful in the design of Pc (or in more general TAP) derivatives for various practical purposes.

Results and Discussion

Synthesis and stability: The yield of 6-*tert*-butyl-2,3-dicyanoanthracene was not high because of the low yield in the last step (Scheme 2). If another dicyanoanthracene such as 2,3-dicyano-9,10-diphenylanthracene could be used, it might be possible to prepare the compound from 2,3-dicyano-7–oxabicyclo[2.2.1]hept-5-ene and 1,3-diphenylisobenzofuran.[9] However, since similar compounds with the same number of the same substituents at similar positions were desired for spectroscopic studies, in order to keep the effect of substituent groups as uniform as possible, it was necessary to choose 6-*tert*-butyl-2,3-dicyanoanthracene, although the route (Scheme 2) is not short (as a substituent, the *tert*-butyl group gives the weakest effects).[10] This route is similar to that used to obtain 6-*tert*-butyl-2,3-dicyanonaphthalene from *o*-xylene.[11]

The metal-free anthracocyanine was very unstable, so spectroscopic data (NMR, absorption, and MCD) were collected as quickly as possible after chromatography, or metal insertion reactions using copper or zinc salts in DMF or V_2O_5 in urea[12] were immediately carried out in the dark under a nitrogen atmosphere. Attempts were also made to synthesize CuAc, VOAc, and CoAc by the so-called nitrile method,[2b,4] but only CoAc was obtained, since CuAc and VOAc decomposed during chromatography. Silica gel or neutral and basic alumina were tested with toluene and toluene/pyridine mixtures as eluents. The use of chloroform, dichloromethane, THF, or their mixtures with methanol or ethanol as eluents was particularly unfavorable, since CuAc and VOAc decomposed in a short time during chromatography.

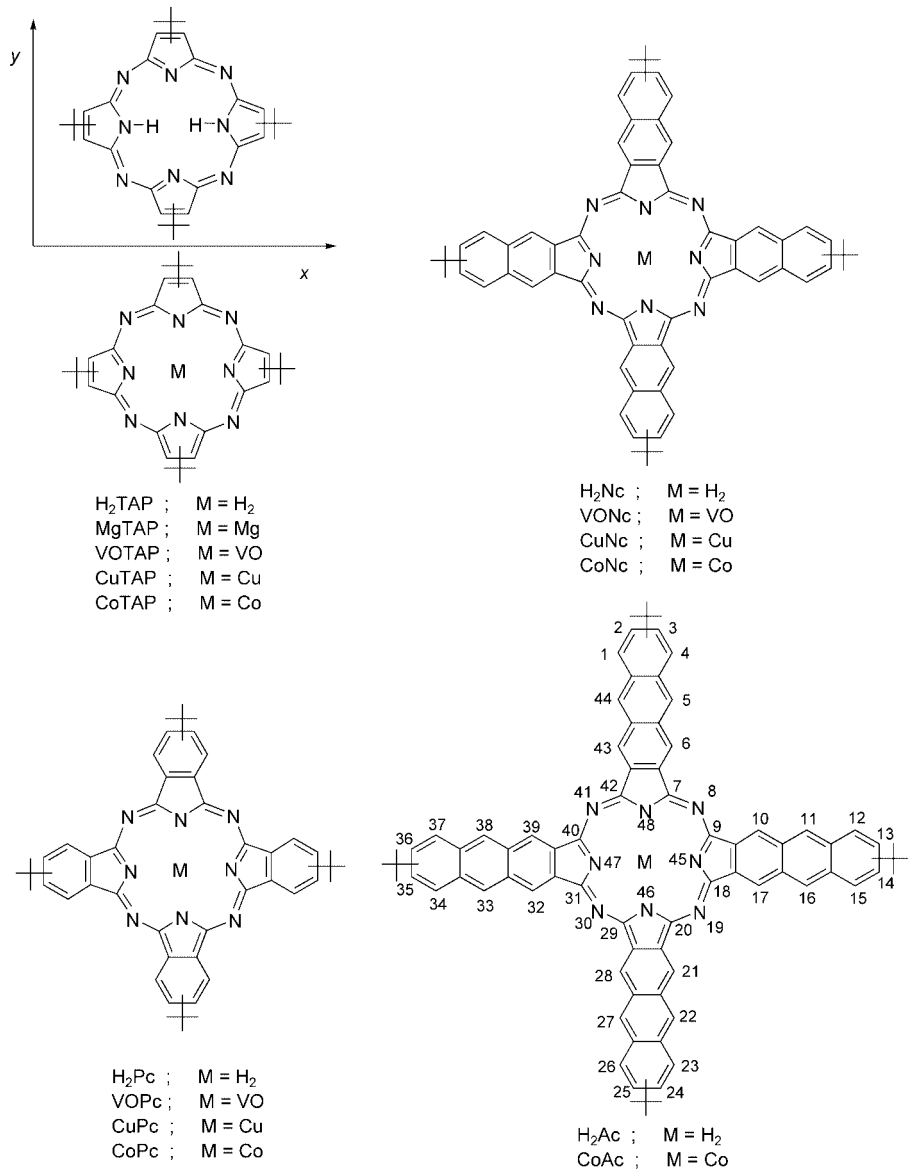

Scheme 1. Structures of and abbreviations for the compounds in this study, and the directions of the *x* and *y* axes. H_2TAP denotes the positions of pyrrole protons as representative of metal-free derivatives.

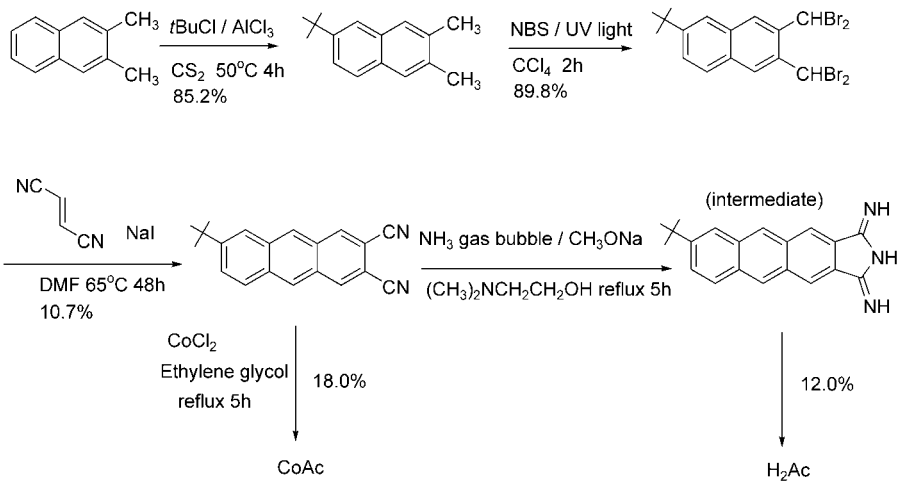

Scheme 2. A synthetic scheme leading to 6-*tert*-butyl-2,3-dicyanoanthracene and CoAc and H_2Ac.

All though CoAc could be stored in the dark for years, solid H_2Ac decomposed within a few days even if stored in the dark under nitrogen. As is discussed later, in the voltammetry section, the stabilities of the compounds appeared to decrease with increasing molecular size, with anthracocyanines being particularly unstable.

Electronic absorption and MCD spectroscopy: The electronic absorption and MCD data of the compounds in pyridine are summarized in Table 1, Table 2, and Table 3. Pyridine was chosen because this was the only solvent to give monomeric spectra for all species. To obtain as quantitative data as possible, analysis was mainly of the Q band. In Table 1, dipole strengths and dipole lengths were estimated by the method of Sauer et al.,[13] whereas the magnetic moments and MCD parameters in Table 2 were obtained by the method of Briat et al.[14] There are of course some experimental errors, but the following results may be extracted from these data.

1) The strength of the Q band—that is, dipole strength, dipole length—generally increases with enlargement of the π system.

2) For each ligand, the Q band intensity of the Cu complexes is always larger than that of the VO complexes (the intensity of Co complexes is not easily compared, since the solvent molecule coordinates at the fifth position), while the Q band of the Cu complexes always lies at shorter wavelength than that of the corresponding VO complexes. The intensity and positional dependence of the Q band on the central metal type has not yet been elucidated. However, this strongly suggests that the central metal dependence of the Q band intensity and position in the Pc series can be maintained even in other ligands. Thus, if the change in intensity and position of the Q band due to the metal type are elucidated with the relatively easily accessible metal Pcs, those in TAPs and Ncs should be deducible from the data for standard TAP and Nc derivatives.

3) MCD intensity per unit absorption (that is, A/D value), a parameter for the magnitude of the orbital angular momentum of the excited state of the ligand, and the absolute value of magnetic moment decrease with increasing size of the π systems. With respect to A/D value and Q band intensity, anthracocyanines showed smaller values, which may be due to their instability, or to the result of saturation in the series, since the rate of change with increasing molecular size decreases or saturates for larger compounds. It is known that the angular momentum of the metal phthalocyanine ring is always less than the angular momentum of the pure phthalocyanine orbital, and that this is due to the delocalization of a central metal d-electron onto a surrounding ligand through the empty $e_g(\pi^*)$ orbital.[15] Taking this into account, the energy difference between the e_g ($d\pi$) orbital and empty e_g (π^*) orbital of the ligand may decrease with annulation of benzene rings to the TAP ligand.

4) The Q band shifts to longer wavelength, but with an extent diminishing with increasing size of the ligand. This can be clearly seen in the data for the cobalt derivatives, in which the Q bands occur at 570, 660, 752, and 832 nm in the order CoTAP, CoPc, CoNc, and CoAc, respectively. If we set the energy difference of the Q band between CoTAP and CoPc at unity,

Table 1. Dipole strength and dipole length in the $Q_{x(0-0)}$ or Q_{0-0} bands.

Compound	λ_{max} [nm] (kcm^{-1})	ε (logε)	Half band width at $1/\varepsilon$ height [cm^{-1}]	Dipole strength [$Debye^2$]	Dipole length [Å]
H_2TAP	619.0 (16.15)	61800 (4.79)	282.1	17.59	0.875
CoTAP	570.0 (17.54)	40600 (4.61)	580.0	21.87	0.975
CuTAP	583.4 (17.14)	73700 (4.87)	360.0	25.25	1.048
VOTAP	594.0 (16.84)	48400 (4.68)	330.0	15.45	0.820
MgTAP	592.0 (16.89)	45300 (4.66)	390.2	17.06	0.861
H_2Pc	698.0 (14.33)	141200 (5.15)	250.0	40.16	1.321
CoPc	660.0 (15.15)	109600 (5.04)	421.5	49.72	1.470
CuPc	676.0 (14.79)	146600 (5.17)	291.3	47.09	1.431
VOPc	698.0 (14.33)	102300 (5.01)	357.5	41.62	1.345
H_2Nc	783.6 (12.76)	202800 (5.31)	260.0	68.38	1.724
CoNc	752.0 (13.30)	152800 (5.18)	293.7	55.02	1.547
CuNc	771.2 (12.97)	225400 (5.35)	299.4	84.85	1.921
VONc	809.6 (12.35)	125900 (5.10)	268.0	44.55	1.392
H_2Ac	858.3 (11.65)	89100 (4.95)	257.5	32.11	1.182
CoAc	831.5 (12.03)	71100 (4.85)	299.3	28.84	1.120

Table 2. Experimental determination of the MCD parameters in the $Q_{x(0-0)}$ or Q_{0-0} bands.

Compound	λ [nm] (kcm^{-1})	Band width at $^1/_2$ height τ [cm^{-1}]	A/D	Magnetic moment (μ)	$[\theta_1]_m$	$[\theta_2]_m$	(dif)	S	B/Dx 10^4	ε_{max}
H_2TAP	619.0(16.15)	369.9			−29.89				+24.763	61800
CoTAP	570.0(17.54)	1221.5	+2.387	−4.774	−30.15	10.12	−40.27	−20.03	+17.119	40600
CuTAP	583.4(17.14)	561.6	+2.945	−5.890	−108.22	87.93	−196.15	−20.29	+9.533	73700
VOTAP	594.0(16.84)	592.7	+3.278	−6.556	−74.79	61.08	−135.87	−13.71	+9.829	48400
MgTAP	592.0(16.89)	563.3	+3.349	−6.698	−72.11	64.60	−136.71	−7.51	+5.753	45300
H_2Pc	698.0(14.33)	372.8			−146.21				+53.017	141200
CoPc	660.0(15.15)	915.0	+1.691	−3.382	−65.33	37.49	−102.82	−27.84	+8.814	109600
CuPc	676.0(14.79)	455.0	+2.539	−5.708	−230.56	184.66	−415.22	−45.90	+10.864	146600
VOPc	698.0(14.33)	589.9	+2.270	−4.540	−119.34	80.53	−199.87	−38.81	+13.164	102300
H_2Nc	783.6(12.76)	470.8	+1.401	−2.802	−187.55	118.70	−306.25	−68.85	+11.781	202800
CoNc	752.0(13.30)	461.8	+1.443	−2.886	−141.00	101.42	−242.42	−39.58	+8.988	152800
CuNc	771.2(12.97)	482.6	+1.493	−2.986	−195.58	158.33	−353.91	−37.25	+5.735	225400
VONc	809.6(12.35)	506.3	+1.446	−2.892	−116.62	65.92	−182.54	−50.70	+13.974	125900
H_2Ac	858.3(11.65)	411.9	+0.372	−0.744	−23.23	17.62	−40.85	−5.61	+2.185	89100
CoAc	831.5(12.03)	433.6	+0.606	−1.212	−23.00	27.41	−50.41	+4.41	−2.152	71100

Table 3. Absorption and MCD of the tetraazaporphyrin derivatives.

Compound	Absorption λ [nm ($\log\varepsilon$)]	MCD λ [nm] ($10^{-4}[\theta]_M$ deg $mol^{-1}cm^{-1}T^{-1}$)
H_2TAP	619.0 (4.79), 592.0 (3.84), 550.5 (4.59), 520.0 (4.02), 334.0 (4.79),	618.0 (−29.89), 590.0 (−4.45), 563.0 (0), 552.0 (26.63), 521.0 (7.63), 343.5 (−8.90), 330.0 (0), 317.0 (4.36)
CoTAP	570.0 (4.61), 530.0 (4.16), 313.0 (4.52)	579.8 (−30.15), 569.0 (0), 527.0 (14.00), 561.0 (10.12), 350.0 (−1.41), 321.0 (−2.14), 304.0 (0)
CuTAP	583.4 (4.87), 535.5 (4.09), 337.0 (4.63)	588.0 (−108.22), 583.5 (0), 579.0 (87.93), 535.5 (17.59), 342.5 (−6.12), 332.0 (0), 318.0 (2.67)
VOTAP	594.0 (4.68), 542.0 (3.96), 343.0 (4.57)	670 (−1.20), 599.0 (−74.79), 593.0 (0), 589.0 (61.33), 544.5 (11.84), 352.0 (−5.16), 339.0 (0), 326.0 (2.24)
MgTAP	592.0 (4.66), 543.0 (3.82), 335.0 (4.41)	599.0 (−72.11), 593.0 (0), 588.0 (64.29), 545.0 (11.12), 390.0 (−0.99), 363.0 (−0.32), 341.5 (−2.85), 329.0 (0), 316.0 (1.44)
H_2Pc	698.0 (5.15), 664.3 (5.11), 640.1 (4.61), 602.0 (4.44), 344.0 (4.84),	696.0 (−145.45), 680.5 (0), 661.5 (76.51), 630.5 (42.42), 603.0 (22.35), 360.0 (−6.70), 342.5 (0), 328.0 (5.98)
CoPc	660.0 (5.04), 599.0 (4.49), 332.0 (4.73)	669.0 (−65.33), 657.0 (0), 648.0 (37.21), 597.5 (28.40), 351.5 (−7.67), 335.0 (0), 326.5 (4.26)
CuPc	676.0 (5.17), 609.0 (4.37), 345.0 (4.59)	683.5 (−230.56), 677.0 (0), 671.0 (184.13), 611.0 (32.02), 360.0 (−5.31), 345.5 (0), 327.0 (3.47)
VOPc	698.0 (5.01), 630.0 (4.32), 350.0 (4.70)	704.5 (−119.63), 697.0 (0), 688.5 (80.53), 630.5 (24.04) 372.0 (−5.21), 351.0 (0), 338.0 (3.74)
H_2Nc	783.6 (5.31), 697.5 (4.53), 746.7 (4.72), 606.5 (3.70), 362.0 (4.52), 505.6 (3.36), 327.3 (4.90)	763.0 (−185.96), 784.5 (0), 777.5 (117.12), 699.5 (41.15), 368.0 (−4.85), 333.0 (0), 318.5 (3.60)
CoNc	752.0 (5.18), 672.5 (4.47), 340.0 (4.89)	757.5 (−140.58), 749.0 (0), 742.0 (101.01), 668.0 (25.46), 369.0 (−6.70), 333.5 (0), 320.5 (3.52)
CuNc	771.2 (5.35), 684.5 (4.62), 336.0 (4.78)	782.0 (−195.58), 773.0 (0), 766.0 (158.75), 689.0 (43.18), 389.0 (−5.52), 340.0 (0), 324.5 (6.86)
VONc	809.6 (5.10), 719.0 (4.35), 365.0 (4.79)	816.0 (−115.77), 807.5 (0), 799.0 (65.49), 719.0 (20.70) 380.0 (−4.23), 351.0 (0), 334.5 (3.38)
H_2Ac	858.3 (4.95), 810.0 (4.38), 764.5 (4.28), 567.0 (3.89), 492.0 (4.14), 352.5 (4.90)	870.5 (−23.15), 862.0 (0), 855.0 (17.54), 765.0 (9.26), 512.0 (1.64), 489.0 (0), 409.0 (−2.60), 399.0 (0), 393.0 (1.59), 360.5 (−0.65), 352.5 (0), 345.0 (0.32)
CoAc	831.5 (4.85), 790.0 (4.19), 739.3 (4.11), 565.0 (3.91), 448.0 (4.26), 363.8 (4.67)	848.0 (−23.06), 837.0 (0), 825.5 (27.29), 741.0 (0.58), 485.0 (1.42), 464.5 (0), 436.0 (−1.06), 401.0 (0), 388.0 (1.05), 377.5 (0), 358.0 (−3.11), 339.0 (0) 336.0 (0.48),

the differences between CoPc and CoNc and between CoNc and CoAc were 0.78 and 0.53, respectively. Although CuAc and VOAc were not obtainable, if the Q band energy between TAP and Pc in each complex was set at unity, the differences between the Pc and Nc ligands fall at 0.80 ± 0.02, together with the results for metal-free derivatives described below.

Figure 1 shows the electronic absorption and MCD spectra of the metal-free species, from which several of the characteristics mentioned above can be recognized. For example, the absorption coefficient increases in the order TAP, Pc, and Nc, although that of Ac was slightly smaller than that of Nc. In addition, the Q band shifts to longer wavelength with annulation of benzene rings, but with decreasing extent with

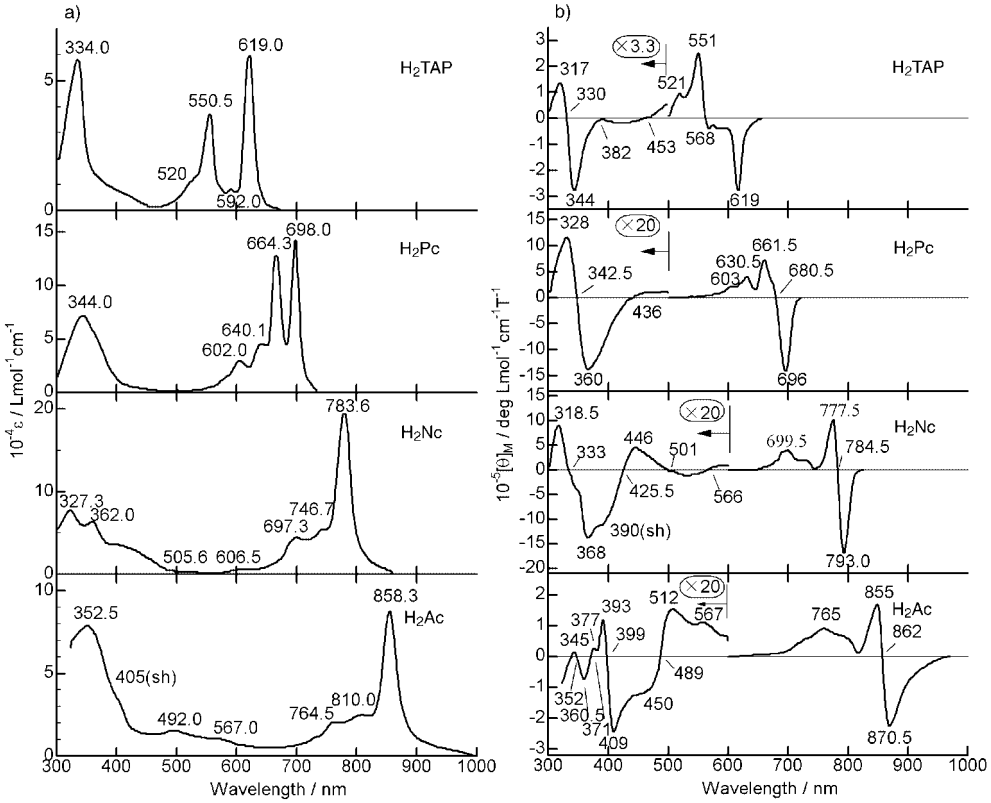

Figure 1. Electronic absorption (a) and MCD spectra (b) of metal-free derivatives in pyridine.

increasing molecular size. If the Q band energy difference between H_2TAP and H_2Pc is set at unity, the differences between H_2Pc and H_2Nc and between H_2Nc and H_2Ac were 0.78 and 0.45, respectively (the Q band position in H_2TAP and H_2Pc was defined as the center of the split peaks). Thus, as an average of metal-free and cobalt derivatives, the effect of increasing the size of the ring system from Nc to Ac was approximately 0.5 ± 0.03 of that from the TAP to Pc ligand. Furthermore, this value illustrates an invaluable fact: the Q bands of H_2Nc and of H_2Ac do not show the split Q band characteristics of metal-free Pcs and porphyrins. We recently reported a linear relationship between the splitting of the Q bands of metal-free Pcs and the wavelengths of the Q bands, for which the splitting was found to decrease for metal-free Pcs with the Q bands at longer wavelengths.[16] Even the observation of splitting for H_2TAP and the absence of splitting for H_2Ac meet this relationship perfectly. Although the reason is not yet elucidated, this effect may happen if the splitting of the LUMO is small, and this is suggested from the results of molecular orbital calculations described later.

The MCD spectra in Figure 1b give additional information. These spectra are essentially composed of Faraday *B* terms, which show MCD peaks or troughs associated with each absorption maximum.[7] The dispersion-type curves seen for the Q bands of H_2Nc and H_2Ac are pseudo-Faraday *A* terms produced by superimposition of close-lying Faraday *B* terms of opposite sign.[17] The minus-to-plus MCD pattern viewing from the lower energy in both the Q and the Soret(B) band regions furthermore indicates experimentally that the splitting of the LUMO is smaller than the splitting between the HOMO and HOMO-1.[18]

Interpretation outside the Q band region is not easy, since many small absorption peaks are observed, while pseudo-Faraday *A* terms are usually seen even in the spectra of normal D_{2h}-type porphyrins and Pcs.[7] From Figure 1, at least two transitions at wavelengths shorter than ca. 470 nm can be recognized for H_2TAP and H_2Pc, while four transitions are discernible in the 300–550 nm region for H_2Nc and in the 300–600 nm region for H_2Ac. H_2TAP appears to have a small absorption at ca. 400 nm. In the case of D_{4h}-type TAPs, the presence of this band had been anticipated already in 1963,[19] and suggested to be attributable to a transition from the lower π orbitals to the doubly degenerate LUMO.[20a] In accordance with this prediction, a Faraday *A* term was detected for *tert*-butylated and phenylated magnesium TAPs.[21a] H_2Pc appears to have a weak absorption at about 400–450 nm, which in the case of metalloPcs can be assigned as the B1 band.[7] However, this band is not clear even in the MCD spectrum. H_2Nc shows absorptions at about 500, 400–470, 362, and 327 nm, and the corresponding MCD spectra are all of the pseudo-Faraday *A*-term type, suggesting that these are all transitions to degenerate or nearly degenerate orbitals. H_2Ac displays three absorption peaks at 567, 492, 353 nm, together with a shoulder at about 400 nm. The strongest MCD signal in this region was found to correspond to this shoulder at ca. 400 nm, and not to the strongest peak at 353 nm. One notable point in the MCD

spectra of H_2Nc and H_2Ac is the presence of negative Faraday *A* term-like curves at 426 nm (H_2Nc) and 489 nm (H_2Ac).

Voltammetry: Figure 2 shows differential pulse voltammograms for VO, Cu, and Co complexes. In the cases of VO and Cu complexes, all couples are ligand-centered, whereas Co derivatives also show couples due to cobalt (for Co derivatives, the assignments are shown in the figure).[22] In all cases at least two oxidation and two reduction couples were observed. With increasing molecular size, the first ligand reduction potential is essentially invariant except in the case of CoPc, but the first ligand oxidation potential shifts to negative, indicating that the LUMO changes only slightly while the HOMO destabilizes significantly. The second ligand oxidation and reduction potentials shift negatively and positively, respectively, with increasing molecular size. For all Co complexes, the Co^{I}/Co^{II} and Co^{II}/Co^{III} redox couples were detected at about -0.5 and $+1.0$ V versus Ag/AgCl, respectively, and the first ligand-reduction potential appeared shifted to more negative potentials than other metal derivatives, since the cobalt is reduced before the ligand and part of the negative charge on cobalt disperses into the ligands. In addition, in contrast to the Cu and VO complexes, the first ligand reduction becomes slightly easier for larger molecules.

Figure 3 summarizes how the "ligand" redox potentials in Figure 2 change depending on the size of the molecule. As can be explicitly seen, the first reduction potential remains almost constant, whereas the first oxidation potential shifts negatively with increasing molecular size, the extent of the shift in the oxidation potential differing from species to species. This suggests that the interaction between the ligand and the central metal differs depending on the metal. In this regard, the shift of the Cu complexes is the largest, and decreases on going to VO and further to Co complexes. One of the most significant points is the molecular size at which

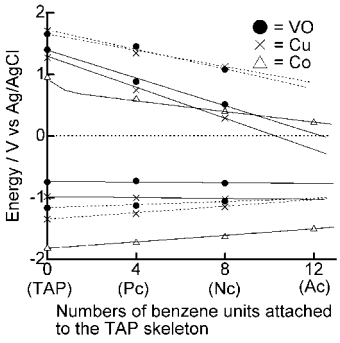

Figure 3. Dependence of "ligand" redox potentials on π-size of macrocycles. The abscissa indicates numbers of benzene units fused to the TAP skeleton. Solid lines: first oxidation and reduction. Broken lines: second oxidation and reduction.

the first ligand-oxidation potential becomes zero. For Cu complexes this occurs when about ten benzene units are fused to the TAP skeleton, which corresponds to a compound intermediate between Nc and Ac. In the case of VO complexes, the number is twelve, which corresponds to Ac. Phthalocyanines are known to be robust—normal CuPc and VOPc without substituents can be recrystallized from concentrated sulfuric acid as solvent—but are decomposed into phthalimide by the action of weak oxidants such as dilute nitric acid.[23] The first oxidation potential of zero volt means that oxidation occurs spontaneously, so this appears to be the reason why the larger TAPs are generally unstable and decompose easily. In the case of Co complexes, this shift toward negative potential is not steep and is still positive for CoAc, so this species can exist stably for years. *The data in Figure 3 strongly suggest that the practical size limit for ring-expanded metalloTAPs is anthracocyanine* (this statement applies for TAP derivatives expanded radially as viewed from the center of the TAP skeleton, and so not for TAP derivatives synthesized from, for example, 1,2-dicyano-

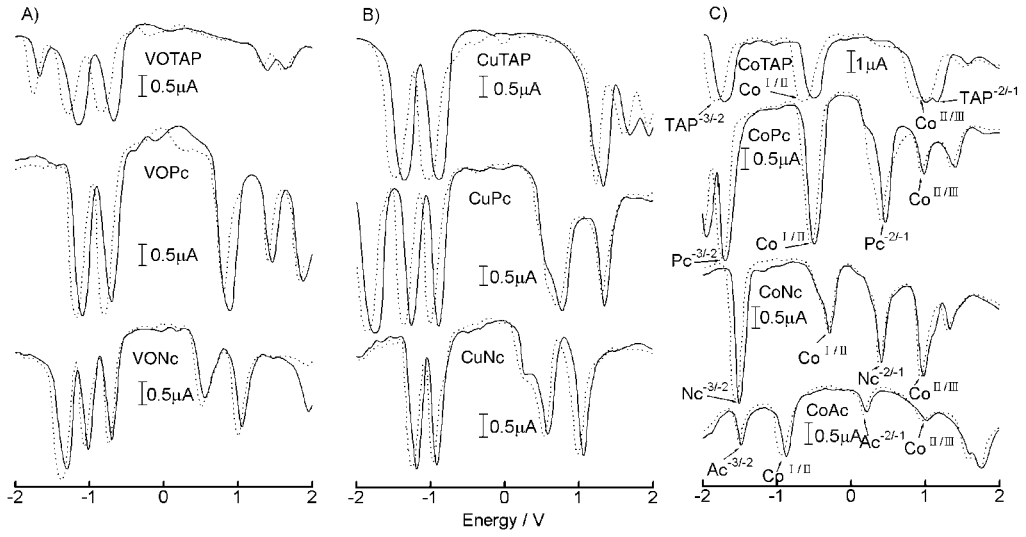

Figure 2. Differential pulse voltammograms of VO (A), Cu (B), and Co (C) complexes in *o*-DCB containing 0.3 mol L^{-1} TBAP. Shoulders appearing at less positive potentials of the first oxidation of the monomeric Cu complexes are due to aggregated species (Cu complexes are prone to aggregation; see, for example, reference [55]).

naphthalene and 1,2-dicyanoanthracene). If tetracenocyanines (Tcs) can exist, it may be as cobalt complexes, or transition metal complexes in which the metal shows redox couples within the potential window.[24] With respect to the possibility of the existence of metallotetracenocyanines (MtTcs), attempts to synthesize copper and vanadyl complexes by the use of 6,12-di(4-*tert*-butylphenyl)-2,3-dicyano-5,11-diphenylnaphthacene under various conditions were made more than 30 years ago. However, the resulting compounds showed the Q band maxima at 780 and 815 nm (solvent not reported), characteristic of naphthalocyanines.[25] In interpretation of this phenomenon, the isomerization of the dinitrile into 2,3-dicyanoisorubrene under the reaction conditions was pointed out.

Spectroelectrochemistry: Spectroelectrochemistry was performed for the Co complexes to determine the redox site and out of spectroscopic interest. Figure 4 shows the spectra of neutral species and those of the first reduction products. Although the spectra of reduced Ncs and Acs have not been reported to date, those of Pcs have been relatively well studied.[7b,c] In the cases of normal CoPcs, it is known that, on reduction of Co^{II}Pcs to form Co^{I}Pcs, the Q band shifts to longer wavelengths with concomitant decrease in intensity and that a new absorption band develops between the Q and Soret(B) bands in the 400–500 nm region, associated with metal-to-ligand charge transfer (MLCT) from cobalt(I) to the Pc ligand.[22,26] Similar behavior has been observed on reduction across the first reduction couple of all Co species in this study, thus indicating that the first reduction couples can be assigned to the $Co^{I/II}$ couple (Figure 2C). Furthermore, analysis of the spectra of these Co^{I} species affords information on the orbital energy. The MLCT band has been assigned as transitions from $e_g(d\pi)$ to the ligand b_{1u} and b_{2u} orbitals using representations under D_{4h} symmetry.[26a] From the energy differences of two peaks in each species (422 and 467 nm for CoPc, 510 and 580 nm for CoNc, and 570 and 674 nm for CoAc), it is suggested that this energy (the difference between the ligand b_{1u} and b_{2u} orbitals) increases with molecular size on going from CoPc (2280 cm^{-1}) to CoNc (2370), and further to CoAc (2710), although that of CoTAP is off this line and is the largest (3460 cm^{-1}). On the other hand, if we tentatively assume that the energy of the $e_g(d\pi)$ orbital is invariant, irrespective of the size of the ligand, then the longer wavelength shift of the MLCT bands with increasing molecular size indicates that the energy difference between the cobalt $e_g(d\pi)$ and ligand b_{1u} and b_{2u} orbitals becomes smaller the larger the ligand size, although CoTAP does not follow this trend. In addition, interestingly, the Q band energy corresponding to the ligand HOMO to LUMO transition does not change with size as much as the neutral Co^{II} species: if the energy difference between CoTAP and CoPc is set at unity, those between CoPc and CoNc and between CoNc and CoAc are 0.86 and 0.77, respectively (in the neutral species, these numbers are 0.74 and 0.54, respectively). Thus, these data suggest that the acquisition of an electron by the central metal does not affect ligand orbitals of different size uniformly. Some of the spectroscopic properties of Co^{I} species can be reproduced in the MO calculations.

Fluorescence and excitation spectra: Fluorescence and excitation spectra with approximate mirror-image relationships in the metal-free species are shown in Figure 5, together with quantum yields (those of H_2Ac are not shown, because it was decomposed by the exciting irradiation). The Stokes shift is generally small, but the values decrease the larger

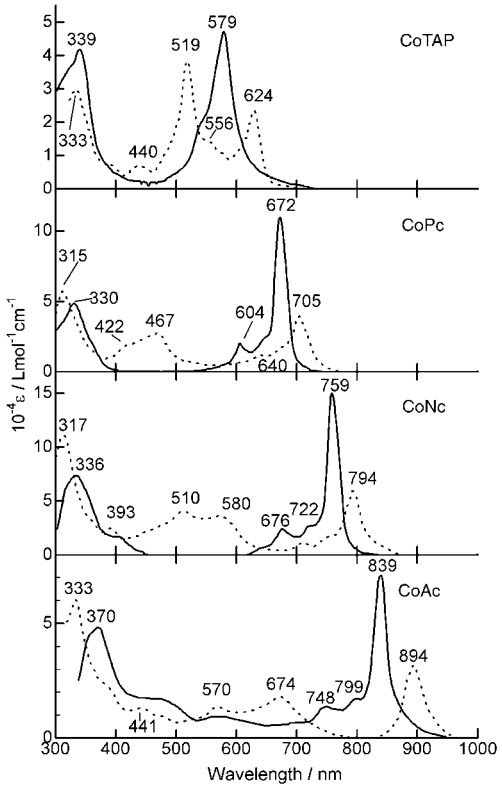

Figure 4. Electronic absorption spectra of Co^{II} (solid lines) and electrochemically reduced Co^{I} species (dotted lines) in *o*-DCB.

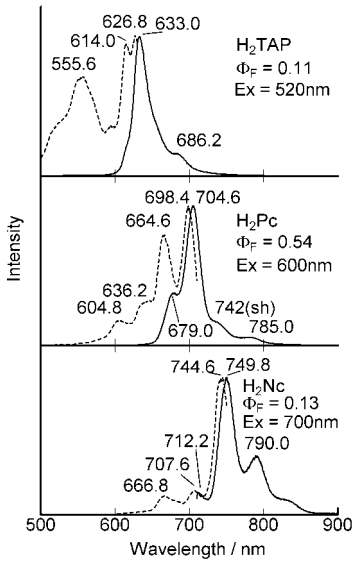

Figure 5. Fluorescence (solid lines) and excitation (dotted lines) spectra of metal-free species in pyridine.

the molecule (156, 114, and 93 cm^{-1} in the order H_2TAP, H_2Pc, and H_2Nc), indicating experimentally that the vibrational level spacing indeed becomes smaller as the size of the π system increases. However, there was no systematic change in the values of Φ_F with size. The value for H_2TAP is similar to that of metal-free tetraphenylporphyrin, having an S_1 emission peak at a similar wavelength, while the value for H_2Nc ($\Phi_F = 0.13$) is much smaller than that of H_2Pc ($\Phi_F = 0.54$). It was recently reported[16] that, among Pcs possessing various substituent groups, Pcs showing emission peaks at shorter wavelengths have higher quantum yields (an almost linear relationship exists) and that Pcs showing S_1 emission maxima at wavelengths longer than about 740 nm generally have quantum yields of less than about 0.1. The Φ_F value of H_2Pc in this study fits this relationship, while the Φ_F value of H_2Nc is also close. In contrast, the Φ_F value for H_2TAP is much smaller and outside this relationship, the reason for which is unclear.

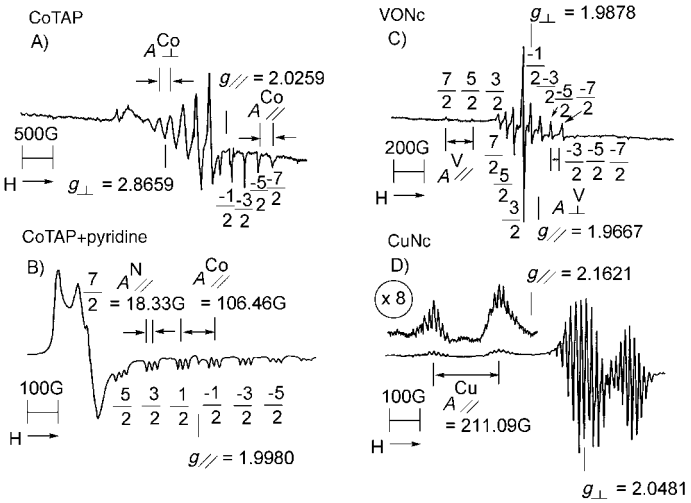

Figure 6. EPR spectra of some metal complexes in toluene at 77 K. A) CoTAP, B) CoTAP + pyridine, C) VONc, and D) CuNc.

Nuclear magnetic resonance: In cases of porphyrinic compounds, NMR spectroscopy gives information on the ring current.[27] In this study, the NMR spectra of metal-free species were compared. Interestingly, the pyrrole proton signals appeared at $\delta = -2.47$, -2.17, -1.64, and -0.73 ppm, while *tert*-butyl protons were detected at 2.18–2.26, 1.88–1.92, 1.78–1.86, and 1.75–1.81 ppm on going from TAP to Pc and Nc, and further to Ac, respectively, indicating that the ring current decreases the larger the macrocycle. This in turn further suggests that the ring current can be explained by a five-orbital model, taking the central TAP core and the surrounding four aromatic moieties into account, rather than a single-orbital model considering a whole molecule as a single loop.

Electron paramagnetic resonance: Although many papers on EPR of paramagnetic porphyrinic compounds have been published, no-one has as yet compared the EPR spectra of π-conjugated compounds of varying size and with the same symmetry. To examine the effect of the π-size, EPR spectra were collected for Co, VO, and Cu complexes, mostly in toluene at 77 K. Figure 6 displays representative spectra, with the data summarized in Table 4. The spectra of non-aggregated CoNc and CoAc could not be obtained, since these showed a marked tendency to aggregate. In particular, it was not possible to disaggregate CoAc even by addition of pyridine, which coordinates to the cobalt.[28]

All cobalt Pcs reported to date adopt a d^7 low-spin, square-planar configuration, with the unpaired electron located in a d_{z^2} orbital.[29] CoTAP and CoPc produced spectra classifiable into this group, as typically shown by the spectrum of CoTAP. For the Co^{II} atom, since $S = {}^1/_2$, $I = {}^7/_2$, and the nuclear-spin quantum number $M_I = \pm{}^1/_2$, $\pm{}^3/_2$, $\pm{}^5/_2$, and $\pm{}^7/_2$, the appearance of two sets of eight lines is to be expected. One set of lines in the low-field region is composed of eight peaks varying in intensity with a separation of 186–268 cm^{-1} (the spacing between the hyperfine (hf) lines is seen to increase with magnetic field). The high-field set consists of six visible weak peaks with a separation of 116–215 cm^{-1} (note that the resonance lines corresponding

Table 4. EPR parameters in toluene at 77 K.

Compound	$g_{\parallel}$	$g_{\perp}$	$10^4 A^{Mt}{}_{\parallel}$	$10^4 A^{Mt}{}_{\perp}$	$10^4 A^{N}{}_{\parallel}$	$10^4 A^{N}{}_{\perp}$
			[cm^{-1}]			
CoTAP	2.0259	2.8659	167.63[a]	235.81[a]		
			min. 117.99	min. 192.00[b]		
			max. 215.31	max. 267.86		
CoPc	2.0244	2.8051	156.69[a]	217.94[a]		
			min. 116.14	min. 186.00[b]		
			max. 197.96	max. 251.06		
CoNc[c]						
CoAc[c]						
CoTAP(py)	1.9980	2.26[b]	99.31		17.10	
CoPc(py)	2.0036	2.34[b]	93.88		17.19	
CoNc(py)	2.0067	2.26[b]	91.24		17.03	
VOTAP	1.9659	1.9889	157.33[a]	53.80[a]		
			min. 155.03	min. 38.43		
			max. 160.28	max. 67.02		
VOPc	1.9652	1.9876	157.60[a]	55.08[a]		
			min. 154.33	min. 40.61		
			max. 159.10	max. 69.82		
VONc	1.9667	1.9878	158.74[a]	54.55[a]		
			min. 156.78	min. 41.03		
			max. 161.35	max. 68.18		
CuTAP	2.1511	2.0472	218.33		15.58	17.11
CuPc	2.1582	2.0479	214.89		15.03	16.43
CuNc	2.1621	2.0485	213.09		15.42	15.73

[a] Average value. [b] Approximate value. [c] Parameters could not be obtained because of aggregation.

to the nuclear transitions $M_I = {}^7/_2$ and ${}^5/_2$ are overlapped by the strong transitions $M_I = -{}^7/_2$ and $-{}^5/_2$ of the low-field multiplet). Although the difference of the $g_\perp$ value of planar low-spin d^7 from 2 is related, to first order, to the gap between the d_{z^2} and d_{xz},d_{yz} orbitals,[29a,30] the two close values for CoTAP and CoPc (Table 4) may reflect that the energy difference between these two orbitals is close in the two systems.

The addition of pyridine to Co systems yielded another type of signal. The hf lines in the parallel (high-field) region split into three lines because of the coordination of pyridyl nitrogen with $I = 1$. As previously predicted theoretically,[31] the $g_\perp$ value approached 2.0, indicating that the energy difference between the d_{z^2} and d_{xz},d_{yz} orbitals had become larger. In the CoTAP, CoPc, and CoNc systems, however, no significant difference in this value is observed, again suggesting that the EPR parameters are similar, in spite of the different ligand size.

The spectrum of VONc is shown as curve C (Figure 6). Similarly to the Co systems, eight hf lines are to be expected due to the magnetic interaction between the V^{4+} unpaired electron ($S = {}^1/_2$) residing in the d_{xy} orbital and the vanadium nucleus of spin $I = {}^7/_2$. The central portion of the spectrum (perpendicular components) is composed of eight closely spaced narrow lines, but with unequal separation (154–161 cm^{-1}). This group of lines is bisected by a strong resonance line due to absorbed oxygen.[32] A second group of lines (parallel components) is composed of five visible peaks, considerably broader and weaker, with unequal separation (38–70 cm^{-1}). As can be seen in the figure, two of these lie at low field and three at high field. The remaining resonance lines belonging to the latter group are completely overlapped by the strong central group (perpendicular components). For all VO complexes, the obtained g values were less than 2 (Table 4), consistently with the theoretical prediction[31a] that the g values of vanadyl complexes possessing an unpaired electron in non-degenerate orbitals are less than 2. Since the unpaired electron in VOPc has been assigned to the d_{xy} orbital,[32] the absence of nitrogen superhyperfine (shf) structure suggests that the electron may be localized on the metal core, and there is little in-plane π bonding. As summarized in Table 4, there is essentially no difference in the EPR parameters of VO complexes of different π size.

Curve D in Figure 6 is the spectrum of CuNc. CuTAP and CuPc also show similar spectra, resembling those reported for copper Pcs reported previously.[33] Since, for the Cu^{II} atom, $S = {}^1/_2$, $I = {}^3/_2$, and the nuclear-spin quantum number $M_I = \pm{}^1/_2$ and $\pm{}^3/_2$, the appearance of two sets of four lines is to be expected. Of the four Cu parallel features, the two at low field show well resolved additional splitting into nine lines, with an intensity ratio of 1:4:10:16:19:16:10:4:1 associated with interaction of the electron with four equivalent nitrogen atoms ($I = 1$). The Cu perpendicular features appearing at high field are also each split into nine lines, which overlap considerably. The shf spacings estimated from the perpendicular components are always larger than those obtained from the parallel components. This difference becomes smaller with increasing molecular size, however, suggesting that there is a trend for magnetic interaction between Cu^{II} and unpaired electrons to become isotropic. The fact that $g_\parallel > g_\perp > 2.0$ for all systems indicates that the unpaired electron is located in the $d_{x^2-y^2}$ orbital.[31a,33c,34] There is little change found in the values of $g_\parallel$ and $g_\perp$ even when the π-size of the ligand is altered.

Infrared spectroscopy and frequency calculations: IR spectra of metal-free and MtPc complexes without peripheral substituents have been studied by several groups.[35] In the case of MtPcs, in-plane vibrations have been classified, by group theory, as X (in-plane $= 14A_{1g}+13A_{2g}+14B_{1g}+14B_{2g}+28_{Eu}$, of which the A_{1g}, B_{1g}, and B_{2g} modes are Raman-active modes, and the E_u mode alone is an IR-active mode. On the other hand, of the out-of-plane modes, X (out-of-plane) $= 6A_{1u}+8A_{2u}+7B_{1u}+7B_{2u}+13E_g$, of which only the A_{2u} mode is IR-active. In the case of metal-free Pcs, the IR-active E_u mode in the D_{4h} molecule splits into B_{2u} and B_{3u} modes, due to lowering of the molecular symmetry to D_{2h}. For MtPcs containing the first transition elements, several vibrations are known to shift from high to low frequencies in the order Ni > Co > Fe > Cu > Zn.[35d] However, the assignments of the fingerprint region have not necessarily been well performed, except for a recent publication employing the DFT method.[36] Of course, only a few reports on the IR of TAPs[37] and Ncs are known.[38] Our compounds in this study are expected to give representative IR data, since they are a series of compounds with similar symmetry but different size.

Experimental data: IR spectra of the compounds used in this study are shown in Figure 7, Figure 8, and Figure 9, together with some calculated spectra. Although the metal-free derivatives gave slightly different spectra, characteristic spectra were obtained in each series. Absorptions originating from

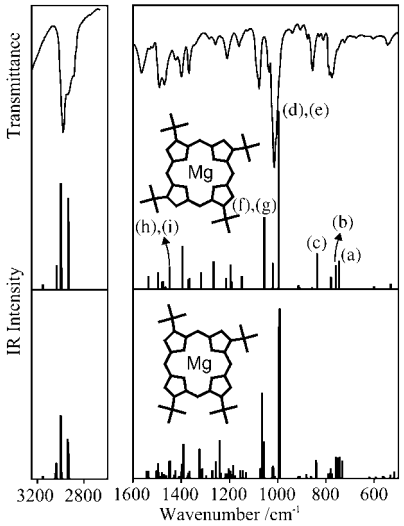

Figure 7. Experimentally measured IR spectrum (KBr, solid line) and calculated frequencies (bars, top: C_{4h} symmetric, and bottom: C_s asymmetric positional isomers) of MgTAP. The skeletal structures are also depicted. Refer to Figure 10 for the selected atomic movements indicated by the letters in the figure.

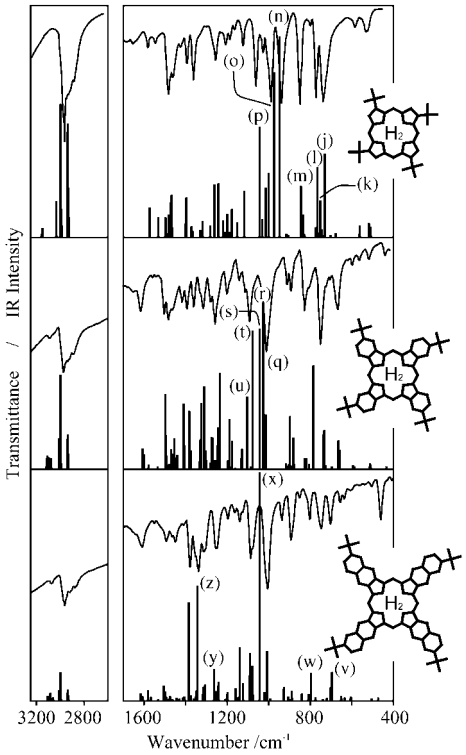

Figure 8. Experimentally measured IR spectra (KBr, solid lines) and calculated harmonic vibrational frequencies (bars) of symmetrically *tert*-butyl-substituted H_2TAP, H_2Pc, and H_2Nc (from top to bottom, respectively). Refer to Figure 10 for the selected atomic movements indicated by the letters.

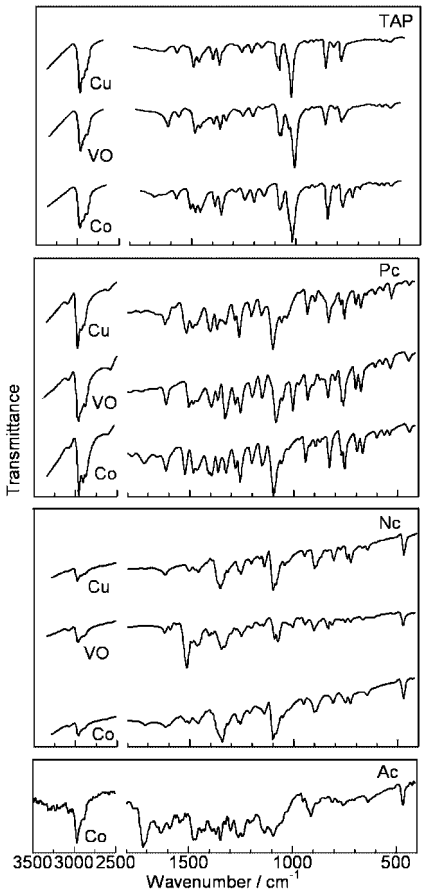

Figure 9. Experimentally measured IR spectra (KBr) of metallo-TAPs, Pcs, Ncs, and Ac (from top to bottom, respectively). Copper, vanadyl, and cobalt (from top to bottom, respectively) derivatives are shown for the first series, whereas only the cobalt complex is given for Ac because of accessibility of the compound.

the *tert*-butyl groups were observed in common for all species—at 2956–2950 (strong, ν_{as}CH), 2904–2910 (medium), 2864–2870 (medium, ν_sCH), 1247–1260 (skeleton), and 1200—1208 cm^{-1} (medium)—while NH stretching vibrations emerged at 3292–3298 cm^{-1} for metal-free species. These vibrations due to *tert*-butyl groups were confirmed by comparison with the IR data for octaphenylated TAPs[39] and substituent-free MtPcs.[35] If we remove the above frequencies attributable to *tert*-butyl groups, the spectra of MtTAPs all contain the following absorptions: 772–777, 843–850, 999–1013, 1064–1078, 1360–1362, 1390–1392, and 1459–1483 cm^{-1}. Of these, those at 999–1013 cm^{-1} were the strongest, and those at 1064–1078 and 1459–1483 cm^{-1} were doublets. Although H_2TAP showed two absorptions at 736 and 940 cm^{-1}, which were not seen for MtTAPs, the above absorptions were also included so that most of these vibrations appeared to originate from the TAP skeletal vibrations.

The spectra of Ncs appear at a glance to be simpler than those of TAPs and Pcs. The absorptions common to all Ncs (except for the aforementioned bands due to *tert*-butyl groups) were seen at 470–472, 724–725, 742–749, 808–812, 888–901, 946–947, 1082–1088, 1100–1104, 1142–1144, and 1343–1359 cm^{-1}. Of these, those at 888–901 and 1343–1359 cm^{-1} were doublet and multiplet, respectively, and those at 1082–1088, 1100–1104, and 1343–1359 cm^{-1} were particularly strong. The bands at 470–472 cm^{-1} were considered to be characteristic of naphthalene,[40] but others may be due to skeletal vibrations. Although the spectra are very similar in shape between CuNc and CoNc, the relative intensities of some VONc bands differed from those displayed by CuNc and CoNc. In addition, the band at 1529 cm^{-1} is of particular note in that it has exceptional strength. The V=O stretching mode[32a,41] observed at 1005 cm^{-1} was weak in VONc, but strong in VOPc. H_2Nc showed a characteristic and strongest band at 1015 cm^{-1}, and its band at 1392 cm^{-1} is more intense than the corresponding band of MtNcs.

The IR spectrum of CoAc, shown in Figure 9, is apparently simpler than those of TAPs and Pcs. Other than vibrations due to *tert*-butyl groups, intense signals were detected at 1717–1703, 1635–1629, 1589, 1480–1460, 1345, 1130–1150, 1091, 909, and 466 cm^{-1}.

Frequency calculations: Although the above IR spectra are somewhat complicated, the recently developed DFT calculation methods satisfactorily succeeded in reproducing the experimentally obtained IR spectra,[36] so that detailed structural analyses are now possible. Therefore, we have extended the analysis to our compounds in order to elucidate the effects of the increase in the size of the ring system. Initially, however, account must be taken of the influence of the existence of the positional isomers on the IR spectra, since the experimentally obtained spectra were recorded on mixtures

of the statistically possible positional isomers. Figure 7 shows the results of frequency calculations of the two positional isomers (top: symmetric C_{4h} and bottom: asymmetric C_s) of MgTAP (bars) together with the experimentally measured spectrum (solid line). Although the symmetric C_{4h} MgTAP shows simpler frequency distributions than the asymmetric species, the two calculated results are, on the whole, similar, indicating that the spectral envelopes are attributable mainly to local structures of the molecule, and that the positional isomers do not significantly affect the shape of the whole spectra. In addition, the resolution of the experimentally obtained spectra is not high enough for the positional isomers to be distinguished, so calculations for the symmetric isomers were undertaken, as shown in Figure 8. The calculated modes were assigned to experimentally observed bands on the basis of both the frequency and the intensity data. In Figure 7, the intense band seen at 1016 cm^{-1}, which is calculated at about 994 cm^{-1}, originates from in-plane motion of the pyrrole nitrogens and pyrrole β-protons (Figure 10 (d), (e)). The moderately intense bands at 1078 cm^{-1} (calculated at ca. 1054 cm^{-1}) have a similar origin ((f), (g)). The band observed at 779 cm^{-1} contains both in-plane (a) and out-of-plane (b) motions over the whole skeleton. On the other hand, the band at 856 cm^{-1} originates exclusively from out-of-plane motion of the pyrrole β-protons (c). A majority of the calculated bands between ca. 1100 and 1600 cm^{-1} are contributed by the *tert*-butyl groups, with the exception of the bands calculated at ca 1446 cm^{-1}, in which the in-plane motion of the skeleton dominates the intensity ((h), (i)).

Figure 8 compares the effects of increasing the size of the ring on a series of metal-free derivatives. In comparison with that of MgTAP, the IR spectrum of H_2TAP has rather complicated spectral envelopes due to the low symmetry of the metal-free derivative. The most intense band, calculated at 945.6 cm^{-1} (n), for H_2TAP originates from the in-plane motion of the central protons, and has of course disappeared in MgTAP. Figure 10 (p) also represents this type of motion. On the other hand, the bands estimated at 842.6 (m) and 971.9 cm^{-1} (o) correspond to the atomic motions depicted in Figure 10 (c) and ((d) (e)), respectively. Similar motions of the pyrrole nitrogens are predicted for H_2Pc (1041.4 cm^{-1} (s)) and H_2Nc (1041.7 cm^{-1} (x)). Out-of-plane motion of the central protons is also characteristic of the metal-free derivatives, as calculated, for example, at 763.4 cm^{-1} (l) for H_2TAP. In the case of H_2Pc, the association between in-plane motion of the central protons and fused benzo protons amplifies the band intensity ((q), (r), (t), and (u)). The in-plane motion at 727.9 (j) and 749.3 cm^{-1} (k) for H_2TAP shifts slightly to 693.6 cm^{-1} (v) for H_2Nc. Most of the other less intense bands calculated for H_2Nc in the energy region between ca. 700 and 900 cm^{-1} originate from the out-of-plane motion of the skeleton, with the exception of the band at 794.6 cm^{-1} (w), which arises from out-of-plane motion of the central protons. H_2Pc has a relatively intense and complicated band distribution in the energy region between about 1100 and 1600 cm^{-1} compared with H_2TAP. This is probably due to the involvement of the fused benzo protons, whereas the association of in-plane motion of the fused naphtho-ring produces an intense characteristic band at 1340.9 (z) and 1382.6 cm^{-1}.

Molecular orbital calculations: *Predicted absorption spectra*: To enhance our understanding of the above spectroscopic and electrochemical data, MO calculations were performed for the metal-free and zinc species since other metals are paramagnetic, for Co^I structures by the ZINDO Hamiltonian, and for the metal-free species also by the PPP Hamiltonian.[20,42–44] Figure 11 displays the calculated spectra, while Table 5, Table 6, and Table 7 summarize details of the calculation results, including the orientations of transition dipoles and configurations. The main results may be summarized as follows:

1) The Q band shifts to longer wavelength with concomitant increase in intensity. However, both the extent of the shift and the increase in the intensity becomes smaller the larger the molecule. If the shift from TAP to Pc is set at unity, the shifts from Pc to Nc and from Nc to Ac were estimated as 0.63 ± 0.05 and 0.49 ± 0.02, respectively, and the calculated relative intensity of the Q band for TAP:Pc:Nc:A*c* = $1{:}1.65 \pm 0.04{:}2.09 \pm 0.06{:}2.33 \pm 0.17$, approximately reproducing the experimental trends.
2) Although the splitting of the Q band of H_2Ac is not necessarily small by the ZINDO/S calculations, if we also judge the results including those by the PPP method (dotted lines in Figure 11 A), the splitting of the Q band decreases on going from TAP to Pc and further to Nc. The splitting in H_2Ac might be slightly larger than that of H_2Nc, since the Q band MCD trough at the longest wavelength is obviously broad (Figure 1 b).
3) Large molecules such as Ncs and Acs have absorptions between the Q and B band arising from transitions from the HOMO to higher empty orbitals. In metal-free compounds, these are found at 506 and 567 nm in H_2Nc and H_2Ac, respectively, whreas for small TAP derivatives, the next highest transition after the Q band is the transition from the low-lying occupied orbital to the LUMO and LUMO+1. Experimentally, H_2TAP showed split transitions at about 420 and 381 nm.[45]
4) The relative intensities of the two MLCT bands in each Co^I species and the relative positions of the MLCT bands among the four Co^I species observed experimentally were reproduced in the calculation. As shown in Figure 4, the longer-wavelength MLCT band shifts to still longer wavelength on going from Co^IPc to Co^IAc, but that of Co^ITAP appeared at a relatively even longer wavelength. This is indeed reproduced. In addition, the larger splitting of the two MLCT transitions of Co^ITAP in relation to other species was also reproduced.

Molecular orbital energy level: Figure 12 shows the calculated energies of some frontier orbitals. The main results may be summarized as follows:

1) The HOMOs of all compounds destabilize with increasing molecular size, but to a decreasing extent, while the LUMOs of the metal-free and zinc derivatives remain

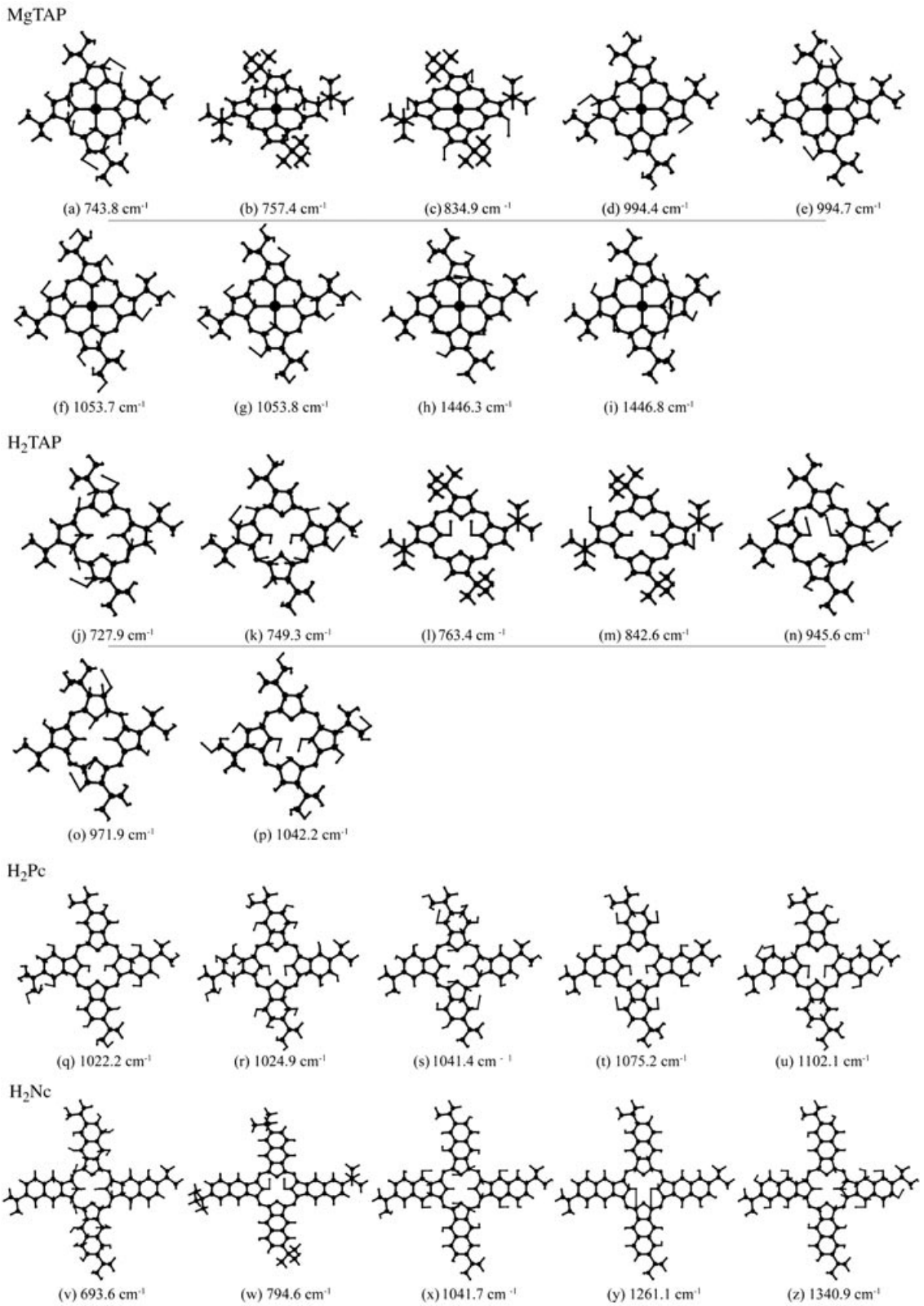

Figure 10. Atomic movements at the selected predicted frequencies.

almost constant in spite of difference in molecular size, reproducing the experimentally found trends in Figure 3.

2) In the case of the cobalt complexes, the destabilization of the HOMO is not as steep as for the metal-free and zinc complexes, while the LUMO stabilizes to some extent with increasing molecular size. As a result, as shown in Figure 3, the first oxidation potential of CoAc is still positive, and the first reduction potential shifts

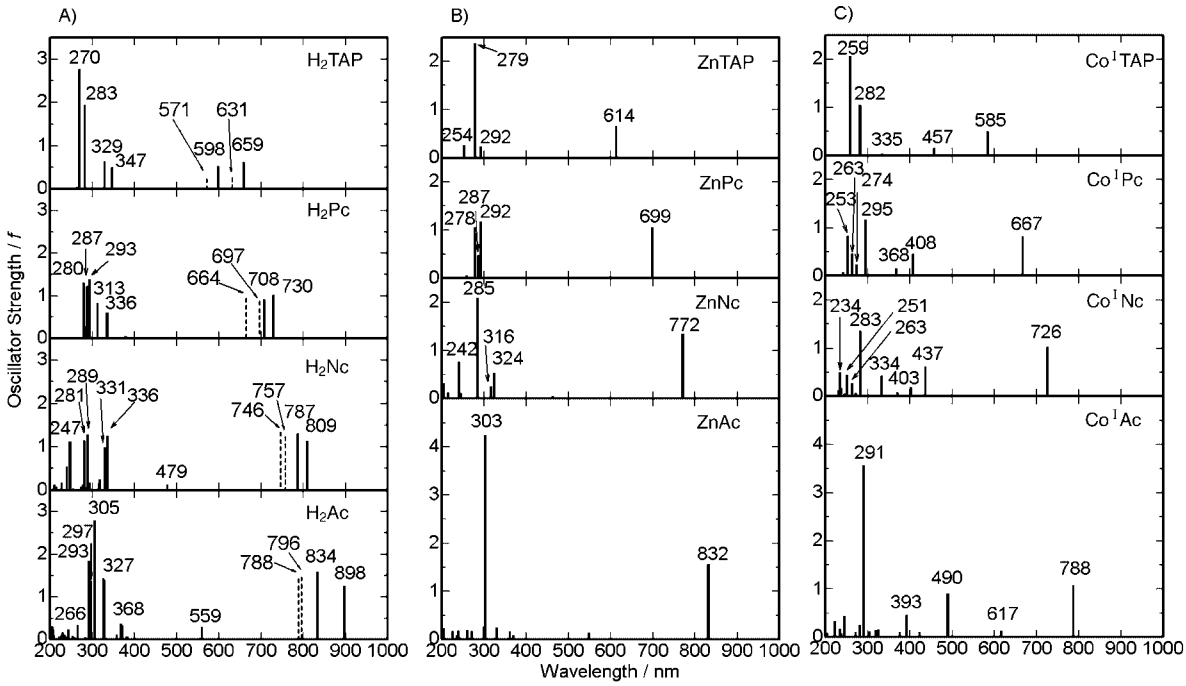

Figure 11. Calculated absorption spectra for: A) metal-free, B) Zn, and C) Co^{I} derivatives of TAP, Pc, Nc, and Ac. In A), broken lines indicate the Q band obtained by use of the PPP Hamiltonian.

positively with enlargement of the macrocycles, in contrast to the metal-free and zinc complexes. Thus, these results are completely consistent with the redox data in Figure 3.

3) In the cases of Ncs and Acs, there are many naphthalene or anthracene-centered orbitals in the frontier orbitals (these are denoted by asterisks in Figure 12).
4) For cobalt complexes, e_g ($d\pi$) orbitals lie as the HOMO−1 and HOMO−2 orbitals and may stabilize slightly for larger molecules (however, in reality, with Co^{I}TAP these $d\pi$ orbitals appear to be the HOMO, since the first reduction product gave a spectrum typical of a Co^{I} complex (Figure 4).
5) A b_{1u} orbital (the LUMO+2 orbital or essentially LUMO+1 orbital, since the LUMO is doubly degenerate) in MtTAP and MtPc (Mt = Zn and Co) stabilizes slightly, while a b_{2u} orbital (the LUMO+3) in the same complexes stabilizes markedly on going from the smaller TAP to the larger Ac, so the order of the b_{1u} and b_{2u} orbitals is inverted in MtNc and MtAc. This explains much of the MLCT band behavior of the cobalt complexes in Figure 4. First, the energy difference between the b_{1u} and b_{2u} orbitals explains the difference of the two peaks in the MLCT band. As seen experimentally (Figure 4), the splitting increases in the order Pc, Nc, Ac, and TAP, and the energy difference between the b_{1u} and b_{2u} orbitals in Figure 12 increases in this order. Second, as can be seen in Figure 12, the fact that the MLCT band shifts to longer wavelength on going from Pc to Nc and further to Ac can be explained by the decrease in the HOMO–LUMO gap due to the marked lowering of the b_{2u} orbital.
6) Concerning point 5, the b_{1g} LUMO and b_{2g} LUMO+1 orbitals in H_2TAP and H_2Pc approach each other in energy on going from H_2TAP to H_2Pc, and in H_2Nc they are almost the same, while their energy is inverted in the larger H_2Ac in both the PPP and ZINDO/S calculations. As a result, the splitting of the two orbitals in H_2Ac becomes larger than that in H_2Nc, which explains the large negative Q MCD envelope at the lowest energy of H_2Ac (Figure 1b).

Conclusion

Through the preparation of a series of TAP derivatives differing only in size, properties that cannot be revealed when treating only one size of compounds emerged. The main results may be summarized as follows.

1) If the shift of the Q band on increasing the size of the ring system from TAP to Pc is set at unity, those from Pc to Nc and from Nc to Ac are about 0.8 and 0.5, respectively. This ratio, however, changes when the oxidation state of the central metal is changed, as seen for Co^{II} and Co^{I} species.
2) The splittings of the Q bands of metal-free species decrease with increasing molecular size, so that the Q bands of H_2Nc and H_2Ac appear as single bands. This is further related to the extent of the shift of the molecular orbital on increasing the size of the ring system. That is, the LUMO+3 b_{2u} orbital in TAP stabilizes markedly, whereas the LUMO+2 b_{1u} stabilizes only slightly when

Table 5. Calculated spectra including orientation of transition dipoles and configurations for metal-free species.[a]

λ [nm]	ν [kcm^{-1}]	f	Obsb.	Pol	Configurations	Assignment
					H_2TAP (MO number 57 is the HOMO)	
659	15.174	0.620	619.0	*y*	57→58 (84%), 56→59 (16%)	Q
598	16.722	0.522	550.5	*x*	57→59 (86%), 56→58 (13%)	Q
347	28.818	0.502		*y*	56→59 (52%), 54→59 (42%)	
329	30.395	0.633		*x*	56→58 (65%), 54→58 (27%)	
283	35.335	1.943	334?	*x*	54→58 (71%), 56→58 (20%)	
270	37.037	2.774		*y*	54→59 (56%), 56→59 (31%)	
					H_2Pc (MO number 93 is the HOMO)	
730	13.698	1.020	698.0	*y*	93→94 (90%)	
708	14.124	0.914	664.3	*x*	93→95 (93%)	
335	29.850	0.602		*y*	92→95 (63%), 90→95 (29%)	
313	31.948	0.837		*x*	92→94 (77%)	
293	34.129	1.393	344?	*y*	93→102 (55%), 90→95 (35%)	
288	34.722	1.233		*x*	90→94 (82%), 93→103 (14%)	
282	35.460	0.288		*x*	93→103 (69%), 92→94 (10%)	
280	35.714	1.317		*y*	93→102 (39%), 90→95 (32%), 92→95 (21%)	
					H_2Nc (MO number 129 is the HOMO)	
809	12.360	1.134	783.6	*x*	129→130 (95%)	
787	12.706	1.317	783.6	*y*	129→131 (92%)	
479	20.876	0.131	505.6	*x*	129→133 (97%)	
336	29.761	1.253		*y*	129→138 (47%), 125→130 (36%)	
331	30.211	0.983		*x*	127→130 (37%), 129→139 (32%), 125→131 (16%)	
318	31.446	0.262		*y*	129→138 (41%), 125→130 (34%), 127→131 (16%)	
316	31.645	0.148		*y*	127→131 (66%), 125→130 (19%)	
295	33.898	0.172		*x*	125→131 (47%), 122→130 (15%), 127→130 (12%)	
289	34.602	1.280		*y*	123→130 (80%)	
281	35.587	1.146		*y*	123→131 (80%)	
278	35.971	0.132		*x*	129→141 (42%) 125→131 (26%), 122→130 (21%)	
247	40.485	1.123		*y*	128→135 (32%), 127→136 (29%), 128→132 (10%), 120→130 (10%)	
240	41.666	0.545		*x*	126→132 (42%), 127→133 (27%), 122→130 (19%)	
					H_2Ac (MO number 165 is the HOMO)	
898	11.135	1.258	858.3	*x*	165→166 (95%)	
834	11.990	1.586	858.3	*y*	165→167 (93%)	
559	17.889	0.293	567.0	*x*	165→169 (93%)	
371	26.954	0.337		*x*	165→174 (68%)	
368	27.173	0.377		*y*	163→167 (43%), 165→175 (24%)	
358	27.932	0.107		*y*	165→175 (41%), 163→167 (31%)	
329	30.395	1.370		*y*	159→166 (28%), 158→166 (26%), 161→167 (14%), 165→179 (10%)	
328	30.487	0.138		*x*	165→178 (63%)	
327	30.581	1.460		*y*	165→179 (41%), 158→166 (16%)	
306	32.679	0.263		*y*	164→170 (21%), 165→179 (19%), 163→171 (17%), 161→167 (16%)	
305	32.786	2.789		*x*	158→167 (42%), 160→170 (14%), 159→171 (14%), 161→166 (13%)	
297	33.670	1.374		*x*	162→168 (23%), 161→169 (16%), 165→178 (14%), 161→166 (13%)	
293	34.129	1.849		*y*	159→166 (48%), 158→166 (22%)	
266	37.593	0.330		*x*	159→167 (32%), 158→167 (17%), 163→169 (15%), 164→172 (11%)	

[a] Excited states with energy less than 5.17 eV and f greater than 0.1 are shown (although some f values are smaller than 0.1).

the ring system is enlarged, so that the energy difference between these orbitals decreases.

3) The magnitudes of the orbital angular momentum of the excited state of the ligand and the magnetic moment decrease with increasing molecular size.
4) The quantum yield of H_2Pc is the largest among the metal-free species, showing no relationship to the molecular size.
5) From the position of the pyrrole proton signals in the ^{1}H NMR spectra, the ring current decreases with increasing molecular size, suggesting that the ring current can be explained by the five-loop model.
6) The first reduction potential changes only slightly with molecular size, while the first oxidation potential becomes markedly less positive, indicating that the HOMO destabilizes significantly as the molecule becomes larger.
7) In 6), the extent of HOMO destabilization with increasing molecular size differs depending on the type of central metal, so that metals showing smaller destabilization can produce larger complexes, since TAPs are unstable against oxidation.
8) The EPR parameters are similar in spite of the differences in the sizes of macrocycles.
9) The IR spectra generally become simpler as the size of the molecule increases, and some of the characteristic bands could be extracted for each size of molecule.
10) Some IR bands characteristic of *tert*-butyl groups and of the TAP, Pc, and Nc skeletons have been assigned on the basis of the DFT calculations.
11) Some of the observed trends in experimentally determined redox potentials and electronic absorption and MCD spectra were reasonably reproduced by use of the ZINDO/S (and occasionally PPP) Hamiltonian(s).

Table 6. Calculated spectra including orientation of transition dipoles and configurations for zinc species.[a]

λ [nm]	ν [kcm^{-1}]	f	Pol.	Configurations	Assignment
				ZnTAP (MO number 57 is the HOMO)	
614	16.286	0.661	x, y	57→58 (87%), 56→59 (12%)	Q
614	16.286	0.661	x, y	57→59 (87%), 56→58 (12%)	Q
292	34.246	0.231	x	55→58 (79%), 51→58 (14%)	
292	34.246	0.231	y	55→59 (79%), 51→59 (14%)	
279	35.842	2.377	x, y	56→58 (73%), 55→58 (10%)	
279	35.842	2.377	x, y	56→59 (73%), 55→59 (10%)	
254	39.370	0.262	x	51→58 (51%), 57→63 (31%)	
254	39.370	0.262	y	51→59 (51%), 57→62 (31%)	
				ZnPc (MO number 93 is the HOMO)	
699	14.306	1.062	x, y	93→94 (93%)	Q
699	14.306	1.062	x, y	93→95 (93%)	Q
292	34.246	1.181	x, y	92→94 (35%), 91→94 (24%), 93→102 (20%), 93→103 (15%)	
292	34.246	1.181	x, y	92→95 (35%), 91→95 (24%), 93→103 (20%), 93→102 (15%)	
287	34.843	0.477	x, y	91→94 (59%), 85→94 (19%)	
287	34.843	0.477	x, y	91→95 (59%), 85→95 (19%)	
278	35.971	1.063	x, y	92→94 (50%), 93→102 (19%) 93→103 (18%)	
278	35.971	1.063	x, y	92→95 (50%), 93→103 (19%) 93→102 (18%)	
				ZnNc (MO number 129 is the HOMO)	
772	12.953	1.343	x, y	129→130 (94%)	Q
772	12.953	1.343	x, y	129→131 (94%)	Q
324	30.864	0.540	x, y	129→138 (76%)	
324	30.864	0.540	x, y	129→139 (76%)	
316	31.645	0.255	x, y	128→130 (77%)	
316	31.645	0.255	x, y	128→131 (77%)	
285	35.087	2.090	x, y	124→130 (45%), 123→130 (18%), 125→131 (14%)	
285	35.087	2.090	x, y	124→131 (45%), 123→131 (18%), 125→130 (14%)	
246	40.650	0.117	x, y	120→130 (59%), 127→132 (10%)	
246	40.650	0.117	x, y	120→131 (59%), 126→132 (10%)	
242	41.322	0.768	x, y	128→134 (23%), 125→131 (19%), 127→132 (18%), 127→133 (15%), 120→130 (12%)	
242	41.322	0.768	x, y	128→135 (23%), 125→130 (19%), 126→132 (18%), 126→133 (15%), 120→131 (12%)	
				ZnAc (MO number 165 is the HOMO)	
832	12.019	1.556	x, y	165→166 (95%)	Q
832	12.019	1.556	x, y	165→167 (95%)	Q
549	18.214	0.138	x, y	165→170 (94%)	
549	18.214	0.138	x, y	165→171 (94%)	
361	27.700	0.156	x, y	165→174 (57%)	
361	27.700	0.156	x, y	165→175 (57%)	
330	30.303	0.242	x, y	165→178 (61%), 164→166 (11%)	
330	30.303	0.242	x, y	165→179 (61%), 164→167 (11%)	
303	33.003	4.238	x, y	160→166 (35%)	
303	33.003	4.238	x, y	160→167 (35%)	
301	33.222	0.272	x, y	161→166 (20%), 163→169 (14%)	
301	33.222	0.272	x, y	161→167 (20%), 162→169 (14%)	
271	36.900	0.173	x, y	159→167 (39%), 159→166 (25%), 160→167 (22%)	
271	36.900	0.173	x, y	159→166 (39%), 159→167 (25%), 160→166 (22%)	
261	38.314	0.200	x, y	161→167 (13%), 163→172 (13%), 153→166 (12%)	
261	38.314	0.200	x, y	161→166 (13%), 162→172 (13%), 153→167 (12%)	

[a] Excited states with energy less than 5.17 eV and f greater than 0.1 are shown (although some f values are smaller than 0.1).

Experimental Section

Measurements: The 500 and 60 MHz ^{1}H NMR and IR spectral measurements were made with JEOL GSX-500, JNM-PM60SI, and Shimadzu FTIR-8100M spectrometers, respectively. Mass spectra were measured with a JEOL SX-102 mass spectrometer (FAB mass) with *p*-nitrophenyl dioctyl ether or *m*-nitrobenzyl alcohol (NBA) as a matrix. Electronic absorption spectra were measured with a HITACHI U-3410 spectrophotometer. Magnetic circular dichroism (MCD) spectra were run on a JASCO J-400X spectrodichrometer in pyridine solutions of ca. 10^{-5}–10^{-6} mol L^{-1}, with a JASCO electromagnet that produces magnetic fields of up to 1.09 T (pyridine was chosen since aggregation appeared the lowest among the solvents tried: $CHCl_3$, CH_2Cl_2, toluene, *o*-dichlorobenzene (DCB), THF, DMF). The magnitude was expressed in terms of molar ellipticity per Tesla, $[\theta]_M$ [10^4 deg mol^{-1} dm^3 cm^{-1} T^{-1}]. Steady-state EPR measurements were carried out at 77 K on a JEOL FE2 XG EPR spectrometer. Spectral grade toluene (Nacalai Tesque Inc.) was used as solvent, and the concentrations of the samples were ca. 0.5×10^{-3} mol L^{-1}. All samples were deaerated by freeze-pump-thaw cycles. Fluorescence and excitation spectra were recorded with a Shimadzu RF-500 spectrofluorimeter with appropriate filters to eliminate scattered light. Fluorescence quantum yields (Φ_F) were determined by use of free-base tetraphenylporphyrin in benzene ($\Phi_F = 0.11$),[46a] tetra-*tert*-butylated tetrabenzoporphyrin in chloroform ($\Phi_F = 0.57$),[46b] or 1,3,3,1′,3′,3′-hexamethylindotricarbocyanine in DMSO ($\Phi_F = 0.28$)[46c] as standards. Data were obtained by a comparative calibration method, by use of the same excitation wavelength and absorbance for the metal-free samples and the calibrants, as well as the same emission energies. All solutions for fluorescence measurements were purged with argon before measurement.

Cyclic voltammetry data were collected with a Hokuto Denko HA-501 potentiostat connected to a Graphtec WX1200 XY recorder. Differential pulse voltammetry data were recorded with a Yanaco P-1100 polarographic analyzer connected to a Watanabe WX 4401 XY recorder. Elec-

Table 7. Calculated spectra including orientation of transition dipoles and configurations for cobalt(I) species.[a]

λ [nm]	ν [kcm^{-1}]	f	Obsb.	Pol.	Configurations	Assignment
					Co^{I}TAP (MO number 61 is the HOMO)	
585	17.094	0.503	624	x, y	61→63 (87%)	Q
585	17.094	0.503	624	x, y	61→62 (87%)	Q
457	21.881	0.156	519	x, y	60→64 (96%)	MLCT
457	21.881	0.156	519	x, y	59→64 (96%)	MLCT
335	29.850	0.040	440	x, y	60→65 (82%)	MLCT
335	29.850	0.040	440	x, y	59→65 (82%)	MLCT
282	35.460	1.046	333	x, y	55→63 (55%), 56→63 (23%), 56→62 (10%)	
282	35.460	1.046	333	x, y	55→62 (55%), 56→62 (23%), 56→63 (10%)	
259	38.610	2.057		x, y	55→62 (38%), 56→63 (33%)	
259	38.610	2.057		x, y	55→63 (38%), 56→62 (33%)	
					Co^{I}Pc (MO number 97 is the HOMO)	
667	14.992	0.814	705	x, y	97→99 (86%)	Q
667	14.992	0.814	705	x, y	97→98 (86%)	Q
436	22.935	0.0029		x, y	96→100 (62%) 95→101 (22%)	MLCT
436	22.935	0.0029		x, y	95→100 (62%) 96→101 (22%)	MLCT
408	24.509	0.448	467	x, y	96→101 (51%), 95→100 (31%)	MLCT
408	24.509	0.448	467	x, y	95→101 (51%), 96→100 (31%)	MLCT
368	27.173	0.148	422	x, y	97→102 (76%)	
368	27.173	0.148	422	x, y	97→103 (76%)	
313	31.948	0.0052		x, y	96→104 (77%)	MLCT
313	31.948	0.0052		x, y	95→104 (77%)	MLCT
295	33.898	1.162	315	x, y	97→107 (30%), 96→104 (14%), 97→106 (12%)	
295	33.898	1.162	315	x, y	97→106 (30%), 95→104 (14%), 97→107 (12%)	
274	36.496	0.241		x, y	91→99 (38%), 97→106 (21%), 92→98 (13%), 88→98 (11%)	
274	36.496	0.241		x, y	91→98 (38%), 97→107 (21%), 92→99 (13%), 88→99 (11%)	
263	38.022	0.466		x, y	91→99 (27%), 92→98 (23%), 96→108 (20%)	
263	38.022	0.466		x, y	91→98 (27%), 92→99 (23%), 95→108 (20%)	
253	39.525	0.827		x, y	96→108 (44%), 92→98 (23%), 96→105 (11%)	
253	39.525	0.827		x, y	95→108 (44%), 92→99 (23%), 95→105 (11%)	
					Co^{I}Nc (MO number 133 is the HOMO)	
726	13.774	1.033	794	x, y	133→135 (92%)	Q
726	13.774	1.033	794	x, y	133→134 (92%)	Q
437	22.883	0.624	580	x, y	132→136 (67%) 133→139 (21%)	MLCT, π–π^*
437	22.883	0.624	580	x, y	131→136 (67%) 133→138 (21%)	MLCT, π–π^*
403	24.813	0.183	510	x, y	132→140 (86%)	MLCT
403	24.813	0.183	510	x, y	131→140 (86%)	MLCT
334	29.940	0.425	393	x, y	133→142 (82%)	
334	29.940	0.425	393	x, y	133→143 (82%)	
283	35.335	1.357	317	x, y	128→134 (42%), 125→135 (21%)	
283	35.335	1.357	317	x, y	128→135 (42%), 125→134 (21%)	
263	38.022	0.276		x, y	123→135 (22%), 132→144 (11%), 124→134 (11%), 120→135 (10%)	
263	38.022	0.276		x, y	123→134 (22%), 131→144 (11%), 124→135 (11%), 120→134 (10%)	
251	39.840	0.455		x, y	123→135 (32%), 125→135 (19%), 124→134 (16%)	
251	39.840	0.455		x, y	123→134 (32%), 125→134 (19%), 124→135 (16%)	
					Co^{I}Ac (MO number 169 is the HOMO)	
787	12.706	1.073	894	x, y	169→170 (47%), 169→171 (45%)	Q
787	12.706	1.073	894	x, y	169→171 (47%), 169→170 (45%)	Q
617	16.207	0.142		x, y	169→175 (71%)	
617	16.207	0.142		x, y	169→174 (71%)	
490	20.408	0.910	674	x, y	168→172 (70%) 168→177 (13%) 169→175 (10%)	MLCT, π–π^*
490	20.408	0.910	674	x, y	167→172 (70%), 167→177 (13%), 169→174 (10%)	MLCT, π–π^*
393	25.445	0.465	570	x, y	168→176 (60%), 169→180 (13%), 168→184 (10%)	MLCT, π–π^*
393	25.445	0.465	570	x, y	167→176 (60%), 169→179 (13%), 167→184 (10%)	MLCT, π–π^*
325	30.769	0.164		x, y	163→172 (24%), 165→170 (14%), 163→173 (11%)	
325	30.769	0.164		x, y	164→172 (24%), 165→171 (14%), 164→173 (11%)	
320	31.25	0.146		x, y	169→183 (13%)	
320	31.25	0.146		x, y	169→182 (13%)	
304	32.894	0.115		x, y	168→177 (47%), 168→172 (13%)	
304	32.894	0.115		x, y	167→177 (47%), 167→172 (13%)	
291	34.364	3.564	333	x, y	160→170 (27%)	
291	34.364	3.564	333	x, y	160→171 (27%)	
281	35.587	0.260		x, y	168→178 (78%)	
281	35.587	0.260		x, y	167→178 (78%)	
246	40.650	0.442		x, y	159→170 (25%), 159→171 (13%), 159→174 (11%)	
246	40.650	0.442		x, y	159→171 (25%), 159→170 (13%), 159→175 (11%)	

[a] Excited states with energy less than 5.17 eV and f greater than 0.1 are shown (although some f values are smaller than 0.1).

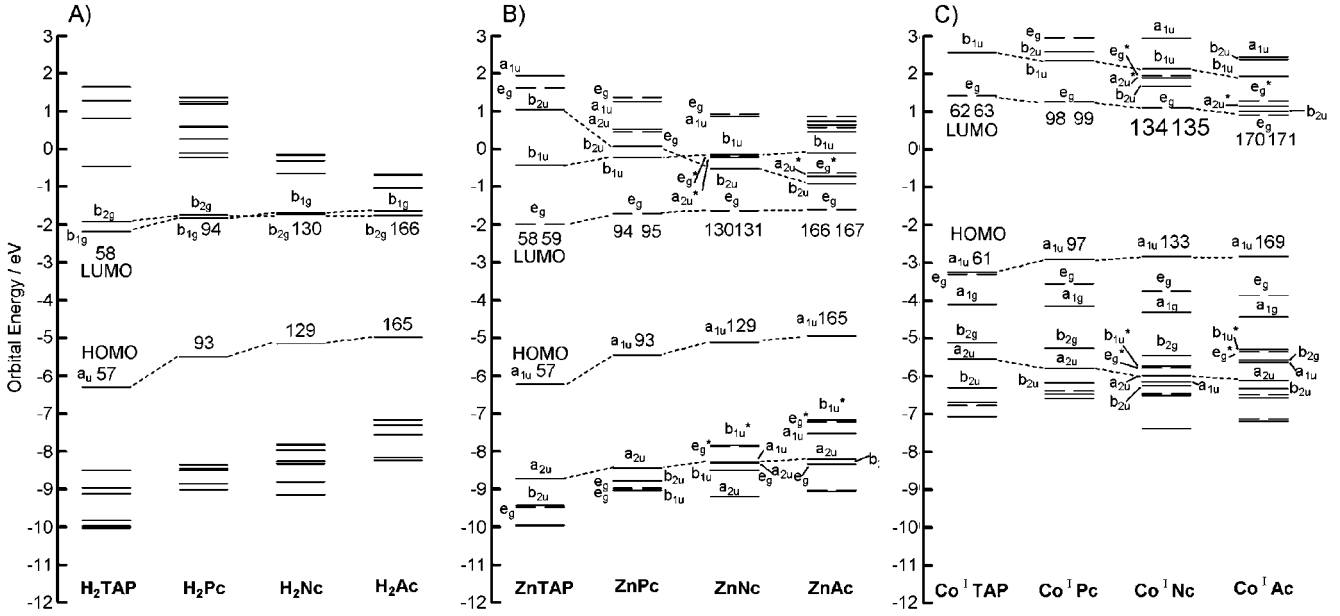

Figure 12. Partial molecular orbital energy diagram for: A) metal-free, B) Zn, and C) Co^{I} derivatives of TAP, Pc, Nc, and Ac, and relationship of some frontier orbitals. Orbitals marked by * indicate naphthalene- or anthracene-centered orbitals. Numbers indicate orbital number. In the orbitals of Co^{I} species, the HOMO−1 and −2 are $e_g(d_{xz},d_{yz})$ orbitals and the HOMO−3 is the a_{1g} (d_{z^2}) cobalt-centered orbital.

trochemical experiments were performed in DCB (Nakalai Tesque, HPLC grade) solution containing tetrabutylammonium perchlorate (TBAP, 0.1 mol L^{-1}) under purified nitrogen. A glassy carbon working electrode (area = 0.07 cm^2), an Ag/AgCl reference electrode, and a Pt wire counter-electrode were employed. For spectroelectrochemical measurements, an optically transparent thin layer electrode (OTTLE) cell of pathlength 1 mm was employed with use of Pt minigrids both as working electrode and as counter-electrode,[47] and a TBAP concentration of 0.3 mol L^{-1}.

Molecular orbital calculations: MO calculations were performed by use of the ZINDO/S Hamiltonian in the HyperChem. R.5.1 program,[43a] and by the PPP Hamiltonian that we have adopted several times previously.[43b] For the PPP calculations, the structures of Pc analogues were constructed from X-ray structural data for standard Pc,[48] naphthalene,[49a] and anthracene[49b] and by making the rings perfectly planar and adopting either the D_{4h} (metallocomplexes) or D_{2h} symmetry (metal-free species), and were therefore essentially the same as those we had used in our previous work.[20] For the ZINDO/S calculations the central metal was assumed to be dihydrogen, zinc, and Co^{I}. The choice of configuration was based on energetic considerations, and all singly excited configurations up to 8 eV (64525 cm^{-1}) were included. The Gaussian 98 program[50] running on a NEC SX-4/128H4 supercomputing system was used to perform DFT calculations. The B3LYP with 6-31G(d) basis set was used for both geometry optimization and frequency calculations. An optimum scaling factor of 0.9613 was applied to the calculated frequencies for comparison with the experimentally obtained data for a Pc.[51]

Materials: H_2-, Cu-, Mg-, VO-,[21a] and CoTAP,[1] H_2Pc,[21b] Co-Pc, Co-Nc, and Co-Ac[1] were the same as used in our previous papers. Commercially available H_2Nc was purified by column chromatography over basic alumina with CH_2Cl_2 as eluent, and was then recrystallized from CH_2Cl_2/MeOH.

Synthesis: Cu-[52a] and VOPc and Cu- and VONc[52b] were obtained by literature methods.

CuPc: Elemental analysis calcd (%) for $C_{48}H_{48}N_8Cu$ (800.49): C 72.02, H 6.04, N 14.00; found: C 72.36, H 6.43, N 14.31.

VOPc: Elemental analysis calcd (%) for $C_{48}H_{48}N_8VO$ (803.89): C 71.72, H 6.02, N 13.94; found: C 72.02, H 6.02, N 13.54.

CuNc: Elemental analysis calcd (%) for $C_{64}H_{56}N_8Cu$ (1000.7): C 76.81, H 5.64, N 11.20; found: C 76.09, H 5.14, N 10.50.

VONc: Elemental analysis calcd (%) for $C_{64}H_{56}N_8VO$ (1004.1): C 76.55, H 5.62, N 11.16; found: C 77.63, H 6.19, N 11.76.

6-*tert*-Butyl-2,3-dicyanoanthracene: A mixture of 6-*tert*-butyl-2,3-dimethylnaphthalene[44] (7.7 g, 36.2 mmol), *N*-bromosuccinimide (28.47 g, 159.7 mmol), and benzoyl peroxide (130 mg, 0.54 mmol) was heated at reflux in CCl_4 (700 ml) with irradiation from a 400 W tungsten lamp for 2 h.[53] The solution was filtered to remove insoluble succinimide, and the solvent was removed on an evaporator. The residue was recrystallized from CCl_4 to give, after drying, 2,3-bis(dibromomethyl)-6-*tert*-butylnaphthalene (15.8 g, 89.8%) as a pale yellow powder (Scheme 2). ^{1}H NMR (60 MHz, $CDCl_3$, 25 °C, TMS): δ = 1.41 (s, 9H), 7.27 (s, 1H), 7.30 (s, 1H), 7.70–8.20 ppm (m, 5H).

This bis(dibromomethyl)naphthalene (8.0 g, 15.2 mmol), fumaronitrile (1.18 g, 15.2 mmol), and sodium iodide (15.2 g, 102.3 mmol) were allowed to react in DMF (50 mL) under nitrogen at 65 °C for two days.[54] After the mixture had cooled, water (300 mL) was added, and the precipitate was collected, dissolved in $CHCl_3$, and washed with sodium thiosulfate ($Na_2S_2O_3$). After removal of the $Na_2S_2O_3$ and $CHCl_3$, the residue was chromatographed over silica gel with toluene as eluent (R_f = 0.2) to give the desired compound (460 mg, 10.7%) as a yellow powder. mp: 216–217 °C; ^{1}H NMR (500 MHz, $CDCl_3$, 25 °C, TMS): δ = 1.47 (s, 9H), 7.80 (dd, 1H), 7.99 (s, 1H), 8.07 (d, 1H), 8.52 ppm (d, 4H); IR: 2970, 2870, 2240 (CN), 1695, 1635, 1482, 1465, 1420, 1378, 1282, 1260, 1103, 1090, 935, 905, 890, 810, 630, 535 cm^{-1}; elemental analysis calcd (%) for $C_{20}H_{16}N_2$(284.35): C 84.48, H 5.67, N 9.85; found: C 84.18, H 5.72, N 9.63.

2,13(or 14),24(or 25),35(or 36)-Tetra-*tert*-butyl-*45H,47H*-anthracocyanine, H_2Ac: An *N,N*-dimethylaminoethanol solution (2 mL) containing 6-*tert*-butyl-2,3-dicyanoanthracene (142.2 mg, 0.5 mmol) was heated at reflux with bubbling of NH_3 gas for 45 min, CH_3ONa (2 mg) was then added, and the reaction was allowed to continue for 5 h. After the mixture had cooled, water was added, and the resulting precipitate was collected by filtration and washed with water and methanol. The residue was chromatographed over alumina with pyridine as eluent to give the desired compound (18 mg, 12%) as a brown powder. This compound was very unstable in air and decomposed within a few days. Accordingly, experiments were carried out under nitrogen as much as possible. ^{1}H NMR (500 MHz, C_5D_5N, 25 °C): δ = −0.73 (s, 2H), 1.75–1.81 (m, 36H), 7.5–8.7 ppm (m, 28H); elemental analysis calcd (%) for $C_{80}H_{66}N_8$ (1139.4): C 84.33, H 5.84, N 9.83; found: C 83.75, H 5.79, N 9.43.

Acknowledgement

This research was partially supported by the Ministry of Education, Culture, Sports, Science, and Technology, Japan, a Grant-in-Aid for the COE project, Giant Molecules and Complex Systems, 2004.

[1] Preliminary results on cobalt complexes have been published: N. Kobayashi, S. Nakajima, T. Osa, *Inorg. Chim. Acta* **1993**, *210*, 131–133.

[2] a) *The Porphyrin Handbook, Vols. 1–10* and *11–20* (Eds.: K. M. Kadish, K. M. Smith, R. Guilard), Academic Press, New York, **1999**, **2003**; b) *Phthalocyanines—Properties and Applications*, *Vols. 1–4* (Eds.: C. C. Leznoff, A. B. P. Lever), VCH, New York, **1989**, **1993**, **1993**, **1996**; c) *The Phthalocyanines* (Eds.: F. H. Moser, A. H. Thomas), *Vols. 1–2*, CRC Press, Boca Raton, FL, **1983**; d) *The Porphyrins*, *Vols. 1–7* (Ed.: D. Dolphin), Academic Press, New York, **1978**; e) *Porphyrins and Metalloporphyrins* (Ed.: K. M. Smith), Elsevier, Amsterdam, **1975**.

[3] *The First International Conference on Porphyrins and Phthalocyanines*, Dijon, France (June 25–30, **2000**).

[4] *Phthalocyanines-Chemistry and Functions* (Eds.: H. Shirai, N. Kobayashi), IPC, Tokyo, **1997**.

[5] N. Kobayashi, J. Mack, K. Ishii, M. J. Stillman, *Inorg. Chem.* **2002**, *41*, 5350–5363, and references [4–8, 20, 43, 46–49] cited therein.

[6] a) N. Kobayashi in *The Porphyrin Handbook, Vol. 2* (Eds.: K. M. Kadish, K. M. Smith, R. Guilard), Academic Press, New York, **1999**, Chapter 13; N. Kobayashi in *The Porphyrin Handbook, Vol. 15* (Eds.: K. M. Kadish, K. M. Smith, R. Guilard), Academic Press, New York, **1999**, Chapter 100; b) N. Kobayashi in *Phthalocyanines—Properties and Applications*, *Vol. 2* (Eds.: C. C. Leznoff, A. B. P. Lever), VCH, New York, **1989,** Chapter 3.

[7] a) M. J. Stillman, T. Nyokong in *Phthalocyanines—Properties and Applications*, *Vol. 1* (Eds.: C. C. Leznoff, A. B. P. Lever), VCH, New York, **1989**, Chapter 3; b) M. J. Stillman in *Phthalocyanines—Properties and Applications*, *Vol. 2* (Eds.: C. C. Leznoff, A. B. P. Lever), VCH, New York, **1989**, Chapter 5; c) J. Mack, M. J. Stillman in *The Porphyrin Handbook, Vol. 16* (Eds.: K. M. Kadish, K. M. Smith, R. Guilard), Academic Press, New York, **2003,** Chapter 103.

[8] E. A. Luk'yanets, *Electronic Spectra of Phthalocyanines and Related Compounds*, NIOPIK, Moscow, **1989**.

[9] C. Schmitz, J. M. Aubry, J. Rigaudy, *Tetrahedron* **1982**, *38*, 1425–1430.

[10] N. Kobayashi, T. Ashida, T. Osa, H. Konami, *Inorg. Chem.* **1994**, *33*, 1735–1740.

[11] K. Ito, H. Uda, N. Kodera, S. Kosuke, H. Kuruma, K. Tanimoto, *Jpn. Patent*, [*Chem. Abstr.* **1969**, *71*, 70299u].

[12] F. Narita, Master Thesis, Tohoku University (Japan), **1998**.

[13] C. Houssier, K. Sauer, *J. Am. Chem. Soc.* **1970**, *92*, 779–791.

[14] B. Briat, D. A. Schooley, R. Records, E. Bunnenberg, C. Djerassi, *J. Am. Chem. Soc.* **1967**, *89*, 7062–7071.

[15] M. J. Stillman, A. J. Thomson, *J. Chem. Soc. Faraday Trans. 2* **1974**, 805–814.

[16] N. Kobayashi, H. Ogata, N. Nonaka, E. A. Luk′yanets, *Chem. Eur. J.* **2003**, *9*, 5123–5134.

[17] a) A. Kaito, T. Nozawa, T. Yamamoto, M. Hatano, Y. Orii, *Chem. Phys. Lett.* **1977**, *52*, 154–160; b) A. Tajiri, J. Winkler, *Z. Naturforsch. Teil A* **1983**, *38*, 1263–1269.

[18] a) J. Michl, *J. Am. Chem. Soc.* **1978**, *100*, 6801–6811 and 6812–6818; b) J. D. Keegan, A. M. Stolzenberg, Y. Lu, R. E. Linder, G. Barth, A. Moscowitz, E. Bunnenberg, C. Djerassi, *J. Am. Chem. Soc.* **1982**, *104*, 4305–4317.

[19] C. Weiss, H. Kobayashi, M. Gouterman, *J. Mol. Spectrosc.* **1965**, *16*, 415–450.

[20] a) N. Kobayashi, H. Konami in *Phthalocyanines—Properties and Applications*, Vol. *4* (Eds.: C. C. Leznoff, A. B. P. Lever), VCH, New York, **1996**, Chapter 9; b) N. Kobayashi, H. Konami, *J. Porphyrins Phthalocyanines* **2001**, *5*, 233–255.

[21] a) N. Kobayashi, S. Nakajima, T. Osa, *Chem. Lett.* **1992**, 2415–2418; b) T. Fukuda, K. Ono, S. Homma, N. Kobayashi, *Chem. Lett.* **2003**, 736–737.

[22] a) W. A. Nevin, W. Liu, S. Greenberg, M. R. Hempstead, S. M. Marcuccio, M. Melnik, C. C. Leznoff, A. B. P. Lever, *Inorg. Chem.* **1987**, *26*, 891–899; b) N. Kobayashi, H. Lam, W. A. Nevin, P. Janda, C. C. Leznoff, A. B. P. Lever, *Inorg. Chem.* **1990**, *29*, 3415–3425.

[23] N. Alessandro, L. Tonucci, M. Bressan, L. K. Dragani, A. Morvillo, *Eur. J. Inorg. Chem.* **2003**, 1807–1814.

[24] A structure of MtTc and the absorption spectrum of the Q band of VOTc were drawn in a paper (W. Freyer, L. Minh, *Monatsh. Chem.* **1986**, *117*, 475–489). Together with the reported Q band maximum (1055 nm), these are all invented data. The authors did not succeed in synthesizing VOTc (this is clearly stated). Moreover, there is a paper that succeeded in reproducing these invented data by molecular orbital calculations (E. Orti, R. Crespo, M. C. Piqueras, F. Tomas, *J. Mater. Chem.* **1996**, *6*, 1751–1761).

[25] V. N. Kopranenkov, E. A. Luk'yanets, *J. Org. Chem. USSR.* **1972**, *8*, 1727.

[26] a) M. J. Stillman, A. J. Thomson, *J. Chem. Soc. Faraday Trans. 2* **1974**, 790–804; b) D. W. Clack, J. R. Yandle, *Inorg. Chem.* **1972**, *11*, 1738–1742; c) W. A. Nevin, W. Liu, M. Melnik, A. B. P. Lever, *J. Electroanal. Chem. Interfacial Electrochem.* **1986**, *213*, 217–234.

[27] a) T. R. Janson, A. R. Kane, J. F. Sullivan, K. Knox, M. E. Kenney, *J. Am. Chem. Soc.* **1969**, *91*, 5210–5214; b) A. R. Kane, J. F. Sullivan, D. H. Kenny, M. E. Kenney, *Inorg. Chem.* **1970**, *9*, 1445–1448; c) T. Koyama, T. Suzuki, K. Hanabusa, H. Shirai, N. Kobayashi, *Inorg. Chim. Acta* **1994**, *218*, 41–45.

[28] Large, flat aromatic molecules are apt to aggregate easily. For example, the aggregation constants of Ncs are much larger than those of the corresponding Pcs. See for example: S. Tai, N. Hayashi, *J. Chem. Soc. Perkin Trans. 2* **1991**, 1275–1279 and S. Tai, N. Hayashi, M. Katayose, *Prog. Surf. Sci. Prog. Surf. Sci. Prog. Org. Coatings,* **1994**, *24*, 323–339.

[29] a) J. M. Assour, W. K. Kahn, *J. Am. Chem. Soc.* **1965**, *87*, 207–212; b) J. M. Assour, *J. Am. Chem. Soc.* **1965**, *87*, 4701–4706; c) J. M. Assour, *J. Chem. Phys.* **1965**, *43*, 2477–2489; d) B. Bleaney, *Philos. Mag.* **1951**, *42*, 441–458.

[30] G. P. Fulton, G. N. La Mar, *J. Am. Chem. Soc.* **1976**, *98*, 2119–2124.

[31] a) B. A. Goodman, J. B. Raynor, *Adv. Inorg. Chem. Radiochem.* **1970**, *12*, 135–362; b) F. A. Walker, *J. Mag. Res.* **1974**, *15*, 201–218.

[32] a) J. M. Assour, J. Goldmacher, S. E. Harrison, *J. Chem. Phys.* **1965**, *43*, 159–165; b) M. Sato, T. Kwan, *J. Chem. Phys.* **1969**, *50*, 558–559.

[33] a) N. Kobayashi, A. B. P. Lever, *J. Am. Chem. Soc.* **1987**, *109*, 7433–7441; b) C. M. Guzy, J. B. Raynor, M. C. R. Symons, *J. Chem. Soc. A* **1969**, 2299–2303; c) J. F. Gibson, D. J. E. Ingram, D. Schonland, *Discuss. Faraday Soc.* **1958**, *26*, 72–80; d) J. S. Griffith, *Discuss. Faraday Soc.* **1958**, *26*, 81–86.

[34] P. W. Lau, W. C. Lin, *J. Inorg. Nucl. Chem.* **1975**, *37*, 2389–2398.

[35] a) I. M. Keen, B. W. Malerbi, *J. Inorg. Nucl. Chem.* **1965**, *27*, 1311–1319; b) A. N. Sidorov, I. P. Kotlyar, *Opt. Spectra* **1961**, *11*, 175–184; c) T. Kobayashi, F. Kurokawa, N. Ueda, E. Suito, *Spectrochim. Acta. Part A* **1970**, *26*, 1305; d) T. Kobayashi, *Spectrochim. Acta. Part A* **1970**, *26*, 1313; e) H. F. Shurvell, L. Pinzuti, *Can. J. Chem.* **1966**, *44*, 125–136; f) T. Onishi, T. Uyematsu, H. Watanabe, K. Tamaru, *Spectrochim. Acta. Part A* **1967**, *23*, 730–732; g) B. Stymne, F. X. Sauvage, G. Wettermark, *Spectrochim. Acta. Part A* **1979**, *35*, 1195–1201.

[36] a) P. Toman, S. Nešpůrek, K. Yakushi, *J. Porphyrins Phthalocyanines* **2002**, *6*, 556–562; b) D. R. Tackley, G. Dent, W. E. Smith, *Phys. Chem. Chem. Phys.* **2001**, *3*, 1419–1426 and **2000**, *2*, 3949–3955; c) T. Fukuda, E. A. Makarova, E. A. Luk'yanets, N. Kobayashi, *Chem. Eur. J.* **2004**, *10*, 117–133; d) N. Kobayashi, T. Fukuda, *Chem. Lett.* **2004**, *33*, 32–33.

[37] a) D. Braun, A. Ceulemans, *J. Phys. Chem.* **1995**, *99*, 11101–11114; b) M. Whalley, *J. Chem. Soc.* **1961**, 866–869.

[38] M. L. Kaplan, A. J. Lovinger, W. D. Reents, Jr, P. H. Schmidt, *Mol. Cryst. Liq. Cryst.* **1984**, *112*, 345–358.

[39] S. Nakajima, Master thesis, Tohoku University, Japan, **1990**.

[40] C. G. Canon, G. B. B. M. Sutherland, *Spectrochim. Acta* **1951**, *4*, 373–395.

[41] S. J. Edmondson, P. C. H. Mitchell, *Polyhedron* **1986**, *5*, 315–317.

[42] a) N. Kobayashi, H. Miwa, V. N. Nemykin, *J. Am. Chem. Soc.* **2002**, *124*, 8007–8020; b) N. Kobayashi, T. Fukuda, *J. Am. Chem. Soc.*

2002, *124*, 8021–8034; c) H. Miwa, E. A. Makarova, K. Ishii, E. A. Luk'yanets, N. Kobayashi, *Chem. Eur. J.* **2002**, *8*, 1082–1090.
[43] a) *HyperChem. R.5.1 Pro*, Hypercube Inc., Gainesville, FL, USA, **1997**; b) N. Kobayashi, H. Lam, W. A. Nevin, P. Janda, C. C. Leznoff, T. Koyama, A. Monden, H. Shirai, *J. Am. Chem. Soc.* **1994**, *116*, 879–890.
[44] N. Kobayashi, T. Ishizaki, K. Ishii, H. Konami, *J. Am. Chem. Soc.* **1999**, *121*, 9096- 9110.
[45] Octaphenylated MgTAP shows this band clearly at 460 nm in pyridine (ref. [21a]).
[46] a) P. G. Seybold, M. Gouterman, *J. Mol. Spectrosc.* **1969**, *31*, 1–13; b) N. Kobayashi, M. Numao, R. Kondo, S. Nakajima, T. Osa, *Inorg. Chem.* **1991**, *30*, 2241–2244; c) J. X. Duggan, J. DiCesare, J. F. Williams, *ASTM Spec. Tech. Publ.* **1983**, *822*, 112–126.
[47] N. Kobayashi, Y. Nishiyama, *J. Phys. Chem.* **1985**, *89*, 1167–1170.
[48] a)J. M. Robertson, I. Woodward, *J. Chem. Soc.* **1937**, 219–230; b) P. A. Barrett, C. E. Dent, R. P. Linstead, *J. Chem. Soc.* **1936**, 1719–1736; c) C. J. Brown, *J. Chem. Soc. A* **1968**, 2488–2493 and 2494–2498; d) J. F. Kirner, W. Dow, W. R. Scheidt, *Inorg. Chem.* **1976**, *15*, 1685–1690.
[49] a) H. O. House, D. G. Koepsell, W. J. Campbell, *J. Org. Chem.* **1972**, *37*, 1003–1011; b) J. P. Fillers, K. G. Ravichandran, I. Abdalmuhdi, A. Tulinsky, C. K. Chang, *J. Am. Chem. Soc.* **1986**, *108*, 417–424.
[50] M. J. Frisch, G. W. Trucks, H. B. Schlegel, G. E. Scuseria, M. A. Robb, J. R. Cheeseman, V. G. Zakrzewski, J. A. Montgomery, Jr, R. E. Stratmann, J. C. Burant, S. Dapprich, J. M. Millam, A. D. Daniels, K. N. Kudin, M. C. Strain, O. Farkas, J. Tomasi, V. Barone, M. Cossi, R. Cammi, B. Mennucci, C. Pomelli, C. Adamo, S. Clifford, J. Ochterski, G. A. Petersson, P. Y. Ayala, Q. Cui, K. Morokuma, D. K. Malick, A. D. Rabuck, K. Raghavachari, J. B. Foresman, J. Cioslowski, J. V. Ortiz, A. G. Baboul, B. B. Stefanov, G. Liu, A. Liashenko, P. Piskorz, I. Komaromi, R. Gomperts, R. L. Martin, D. J. Fox, T. Keith, M. A. Al-Laham, C. Y. Peng, A. Nanayakkara, M. Challacombe, P. M. W. Gill, B. Johnson, W. Chen, M. W. Wong, J. L. Andres, C. Gonzalez, M. Head-Gordon, E. S. Replogle, J. A. Pople, *Gaussian 98*, *Revision A.9*, Gaussian, Inc., Pittsburgh, PA, 1998.
[51] M. W. Wong, *Chem. Phys. Lett.* **1996**, *256*, 391–399.
[52] a) S. A. Mikhalenko, S. V. Barkanova, O. L. Lebedev, E. A. Luk′yanets, *J. Gen. Chem. USSR. Zh. Obshch. Khim.* **1971**, *41*, 2735; b) E. I. Kovshev, V. A. Punchnova, E. A. Luk′yanets, *J. Gen. Chem. USSR.* **1972**, *42*, 691.
[53] W. Ried, H. Bodem, *Chem. Ber.* **1956**, *89*, 708–712.
[54] M. L. Kaplan, A. J. Lovinger, W. D. Reents, P. H. Schmidt, *Mol. Cryst. Liq. Cryst.* **1984**, *112*, 345–358.
[55] N. Kobayashi, H. Miwa, H. Isago, T. Tomura, *Inorg. Chem.* **1999**, *38*, 479–485.

Received: March 22, 2004
Published online: November 3, 2004

